Sociosexual behavior requires both activating and repressive roles of Tfap2e/AP-2ε in vomeronasal sensory neurons

Jennifer M. Lin[1,2], Tyler A. Mitchell[1,2], Megan Rothstein[3], Alison Pehl[1,2], Ed Zandro M. Taroc[1,2], Raghu R. Katreddi[1,2], Katherine E. Parra[4], Damian G. Zuloaga[4], Marcos Simoes-Costa[3], and Paolo E. Forni[1,2,*]

[1]Department of Biological Sciences, University at Albany, Albany, NY, USA.

[2]The RNA Institute, University at Albany, Albany, NY, USA.

[3]Department of Molecular Biology and Genetics, Cornell University, Ithaca, New York 14850, USA

[4]Department of Psychology, University at Albany, Albany, NY, USA.

*Corresponding Author

SUMMARY

Neuronal identity dictates the position in an epithelium, and the ability to detect, process, and transmit specific signals to specified targets. Transcription factors (TFs) determine cellular identity via direct modulation of genetic transcription and recruiting chromatin modifiers. However, our understanding of the mechanisms that define neuronal identity and their magnitude remains a critical barrier to elucidate the etiology of congenital and neurodegenerative disorders. The rodent vomeronasal organ provides a unique system to examine in detail the molecular mechanisms underlying the differentiation and maturation of chemosensory neurons. Here we demonstrated that the identity of postmitotic/maturing VSNs and vomeronasal dependent behaviors can be reprogrammed through the rescue of AP-2ε expression in the AP-2ε^{Null} mice and by inducing ectopic AP-2ε expression in mature apical VSNs. We suggest that the transcription factor AP-2ε can reprogram VSNs bypassing cellular plasticity restrictions, and that it directly controls the expression of batteries of vomeronasal genes.

KEYWORDS

Vomeronasal, Transcription Factor, Tfap2e/AP-2ε, Neuronal Identity, Single-Cell Sequencing, scRNA-seq, CUT&RUN, Chromatin Architecture, Cellular Plasticity, behavior, basal vomeronasal sensory neurons, accessory olfactory bulb, differentiation

INTRODUCTION

Neuronal differentiation is controlled by the selective expression of transcription factors (TFs), chromatin modifiers, and other regulatory factors that reduce cellular plasticity. During neuronal differentiation terminal selectors can activate identity-specific genes that define functional properties specific to a particular neuronal type. However, reprograming postmitotic neurons by ectopically expressing terminal selectors in *C. elegans* suggests that the "reprogrammability" of neurons is progressively lost during postembryonic life (Patel and Hobert, 2017; Patel et al., 2012; Rahe and Hobert, 2019). This reduction in cellular plasticity may arise from chromatin modifications that prevent the activation of alternative differentiation programs. However, sensory neurons of the vomeronasal organ in rodents can undergo some postnatal reprogramming following the aberrant expression of transcription factors (Lin et al., 2018).

The accessory olfactory system (AOS) contains the vomeronasal organ (VNO), which is primarily responsible for detecting odors and chemosignals that trigger social and sexual behaviors (Trouillet et al., 2019; Trouillet et al., 2021). The vomeronasal sensory epithelium of rodents is mainly composed vomeronasal sensory neurons (VSN). The VSN populations selectively express only one or two receptors encoded by the two vomeronasal receptor (VR) gene families: V1R and V2R (Dulac and Axel, 1995; Herrada and Dulac, 1997; Matsunami and Buck, 1997; Ryba and Tirindelli, 1997). V1R and V2R-expressing neuronal populations each detect distinct chemosignals, induce different innate behaviors, show distinct localization patterns in the VNO, and project to specific areas of the accessory olfactory bulb (AOB) (Cloutier et al., 2002; Dulac and Axel, 1995; Isogai et al., 2011; Katreddi and Forni, 2021; Mohrhardt et al., 2018; Mombaerts et al., 1996; Stowers et al., 2002). The V2R-expressing neurons localize to the basal portions of the vomeronasal epithelium (VNE) and around the vasculature (Naik et al., 2020), while V1R-expressing neurons localize to the apical part. Basal and apical VSNs continually regenerate from common pools of Achaete Scute like-1 (Ascl-1)-positive neural progenitor cells (NPCs) localized in the lateral and basal margins of the VNE (Cau et al., 1997; de la Rosa-Prieto et al., 2010; Katreddi and Forni, 2021; Martinez-Marcos et al., 2000; Murray et al., 2003). However, we are only starting to understand how the apical and basal VSN cell differentiation programs are initiated and which factors aide in

maintaining apical and basal neuronal identity (Enomoto et al., 2011; Katreddi et al., 2021; Lin et al., 2018; Naik et al., 2020; Oboti et al., 2015).

Establishing functional basal and apical VSNs is crucial for intra- and interspecies social interactions in rodents. Deficits in basal neuron functionality prevented sex discrimination, reduced male-male and maternal aggressive behaviors, and inhibited the detection of predator odors (Chamero et al., 2011; Stowers et al., 2002).

Transcription factors can drive cellular processes that control the expression of genes defining their cellular and functional identity. The AP-2 family of transcription factors is comprised of 5 members AP-2α, AP-2β, AP-2γ, AP-2δ and AP-2ε, which are encoded by distinct genes (TFAP2A, TFAP2B, TFAP2C, TFAP2D, TFAP2E) (Eckert et al., 2005; Pellikainen and Kosma, 2007; Wankhade et al., 2000). AP-2 family members play critical roles during development, such as contributing to neural crest differentiation (Luo et al., 2020; Rothstein and Simoes-Costa, 2020), cell specification, limb development, and organogenesis (Bassett et al., 2012; Chambers et al., 2019; Kantarci et al., 2015). Some AP-2 family members may have pioneer factor properties (Fernandez Garcia et al., 2019; Rothstein and Simoes-Costa, 2020; Seberg et al., 2017; Williams et al., 2009).

Aside from the AP-2 family, Bcl11b and Tfap2e/AP-2ε control Gαo+ VSNs' differentiation and survival (Enomoto et al., 2011). We proposed that AP-2ε, which is only expressed after the apical and basal VSN dichotomy is established, is necessary for further specification of basal VSN identity (Lin et al., 2018). Using mice expressing non-functional AP-2ε, we discovered that VSNs can still acquire the Gαo+/basal identity; however, these VSN have reduced survival and can acquire some Gαi2+/apical VSNs molecular features over time (Lin et al., 2018). While we examined the role of AP-2ε in maintaining cellular identity and homeostasis of the vomeronasal epithelium, critical outstanding questions remain unresolved. What role does this transcription factor actively play to control the basal genetic program? What is the extent of cellular plasticity in differentiated neurons in mammals (Patel and Hobert, 2017; Rahe and Hobert, 2019)?

Here, we aimed to understand 1) if AP-2ε functions as a terminal selector factor for basal VSNs, 2) how much cellular plasticity postmitotic neurons retain once differentiated, and 3) to what extent genetic dysregulation in mature VSNs translates into

behavioral changes. We generated a Cre inducible mouse line, where we inserted the mTfap2e/AP-2ε gene into the ROSA26 locus. Using this knock-in mouse line, we could 1) rescue the AP-2ε KO's VNO morphology and functionality and 2) ectopically express AP-2ε in maturing Gαi2+/apical VSNs. This approached enable us to assess its ability to reprogram differentiated apical VSNs to basal VSNs. By combining histological analyses, behavioral assessments, and single-cell RNA sequencing (scRNA-seq) analysis, we examined whether AP-2ε functioned as a master regulator to reprogram differentiated neurons and alter animal behaviors. In addition, we used CUT&RUN (Skene et al., 2018) to identify direct genetic targets of AP-2ε that controls the basal VSNs identity program. Overall, we suggest that AP-2ε partially functions as a terminal selector for basal VSN neuronal identity by activating some basally enriched genes while simultaneously suppressing specific apically enriched genes.

RESULTS

Transcriptome differences between apical and basal VSNs

Using single cell RNA-sequencing (scRNA-Seq) on VNOs from OMPCre+ control mice at P10, we identified key features of VSNs based on the expression plots. We then clustered single cells into representative UMAPs (Figure 1). Ascl1(Figure 1A), Neurogenin1 (Neurog1) (Figure 1B), and NeuroD1 (Figure 1C) expression identified proliferative VSN progenitors (Katreddi and Forni, 2021). We determined that the dichotomy of apical-basal differentiation begins when the cells transition from Neurog1 to NeuroD1 expression, and during the NeuroD1 phase (Figure 1B,C)(Katreddi et al., 2021). The later stages of apical and basal VSN maturation were marked by the expression of Gap43 (Figure 1D) in immature neurons and OMP (Figure 1E) in more mature VSNs (Katreddi and Forni, 2021).

Consistent with prior reports, Bcl11b was expressed in Neurog1/NeuroD1 precursors and in differentiating apical and basal VSNs. While Bcl11b was expressed as a continuum along the basal differentiation trajectory, Bcl11b was not expressed in the apical neurons until later stages of maturation (Figure 1F, (Enomoto et al., 2011; Katreddi et al., 2021)). The transcription factor Meis2 was expressed in progenitor cells, and differentiating and maturing apical neurons, but not in differentiating basal VSNs (Figure

1G). In addition, Tfap2e/AP-2ε (Figure 1H) was expressed in maturing and mature basal VSNs after the apical-basal differentiation dichotomy was established, in line with our prior work (Lin et al., 2018). Using scRNA-Seq between mature (OMP+) apical and basal VSNs, we confirmed the differential expression of known markers for either apical or basal VSNs (e.g. Meis1, Meis2, Gnai2/Gαi2, and Nrp2 for apical and Gnao1/Gαo, Tfap2e/AP-2ε, and Robo2 for basal). However, we also identified numerous unreported genes that were significantly enriched in apical and basal VSNs ($q<0.05$, Figure 1J, Supplementary Table S1). Among these, we validated Keratin18 (Krt18) as a novel marker for basal VSNs using histochemistry (Figure1J, Figure2K-M).

Inducible R26AP2ε rescues basal VSNs in AP-2ε KOs

We hypothesized that Tfap2e (AP-2ε) can control gene expression during basal VSN maturation. So, we generated a new Cre inducible mouse line (B6.Cg-Gt(ROSA)26Sor$^{tm(CAG-mTfap2e)For}$). We inserted a lox-P-flanked stop cassette to prevent the transcription of a CAG promoter driven murine Tfap2e gene, which was knocked into the first intron of the Gt(ROSA)26Sor locus (Figure 2A). We refer to this as R26AP2ε. AP-2ε expression is normally restricted to basal regions of the VNO with higher expression levels of AP-2ε in the neurogenic marginal zones (Enomoto et al., 2011; Lin et al., 2018; Naik et al., 2020)(Figure 2 B,B'). To test our Cre inducible AP-2ε line, we performed anti-AP-2ε immunostaining on wild-type controls, AP-2ε$^{Cre/Cre}$ (AP-2ε^{Null})(Feng et al., 2009; Lin et al., 2018), and AP-2ε$^{Cre/Cre}$ /R26AP2ε (AP-2ε^{Rescue}) mice (Figure 2B-D). As expected, wild-type mice showed AP-2ε immunoreactivity in the basal regions of the VNE with strong immunoreactivity in proliferative regions (Figure 2B, B'). However, in AP-2ε^{Null} mice, where Cre was knocked into the DNA binding domain of AP-2ε (Feng et al., 2009; Feng and Williams, 2003), we observed faint AP-2ε cytoplasmic immunoreactivity limited to the most marginal zones of the VNO and no immunoreactivity in the rest of the neuroepithelium (Figure 2C, C'). AP-2ε^{Rescue} mice showed restored AP-2ε immunoreactivity in the basal region of the VNE. However, we observed that the AP-2ε expression pattern and immunoreactivity were not identical to controls in the neurogenic regions. In AP-2ε^{Rescue} mice, we observed no AP-2ε immunoreactivity at the tips of the

neurogenic niche in the VNE (Figure 2D'), suggesting a delayed AP-2ε expression after AP-2εCre mediated recombination compared to controls (Figure 2B',D').

By analyzing the expression of the basal markers downregulated in AP-2ε KOs (Lin et al., 2018), such as V2R2 (Figure 2E-G) and Gαo (Figure 2H-J), we confirmed restored expression in the rescued KOs. Cell quantifications indicated a significant increase in the number of basal cells expressing basal markers in AP-2ε^{Rescue} compared to AP-2ε^{Null} mice, though the number of basal VSNs in the AP-2ε^{Rescue} was smaller when compared to controls. Keratin18 (Krt18) is normally enriched in basal neurons (Figure 1J). Immunohistochemistry confirmed Krt18 protein expression in the basal territories of the VNO (Figure 2K). We observed reduced Krt18 immunoreactivity in AP-2ε^{Null} mice and restored expression in AP-2ε^{Rescue} mice (Figure 2L-N). However, in AP-2ε^{Rescue} mice, Krt18 still showed lower expression levels than in WT mice (Figure 2N). Taken together, we conclude that exogenous AP-2ε in postmitotic VSNs can partially rescue the expression of basal VSN markers in AP-2ε^{Nulls} mice. Rescue of the AP-2ε^{null} phenotype indicates that our inducible R26AP2ε mouse line is a suitable model for conditional expression of functional AP-2ε.

Re-expressing AP-2ε in AP-2ε mice rescues social behaviors

The specification and organization of VSNs and their respective circuit assembly in the AOB are essential to trigger a variety of social and sexual behaviors (Chamero et al., 2011; Chamero et al., 2007; Stowers et al., 2002; Trouillet et al., 2019) . We speculated that AP-2ε^{Null} mice could not discriminate between urine of different sexes. Thus, we performed an odorant preference test. In this test, individual mice were simultaneously presented with male and female whole urine for a two-minute period (Figure 3A). Wild-type mice showed a significant preference for urine from the opposite sex (Figure 3B)(Pankevich et al., 2004; Stowers et al., 2002). However, AP-2ε^{Null} male mice did not display significant preference for female urine, confirming a loss of function (LOF) of basal VSNs (Lin et al., 2018) and consequently a reduced ability to discriminate between urine from either sex (Figure 3B)(Pankevich et al., 2004; Stowers et al., 2002).

However, AP-2ε^{Rescue} male mice showed a significant preference for female urine similar to WT controls (Figure 3B).

To further investigate the behavioral outcome of AP-2ε LOF and AP-2ε re-expression in AP-2ε^{Null} mice, we performed a resident intruder assay for intermale aggression (Figure 4C)(Chamero et al., 2011; Montani et al., 2013; Stowers et al., 2002). Wild-type male mice showed aggressive behaviors toward intruders upon detecting male specific odorants (Figure 4D). Most AP-2ε^{Null} mice did not attack the intruder (Figure 3D). Yet, when male AP2$\varepsilon^{Cre/Cre}$/R26AP2$\varepsilon^{+/-}$ (AP-2ε^{Rescue}) mice were exposed to male intruders, they displayed aggressive behavior similar to that of controls (Figure 3D). We measured the mass of the seminal vesicles from each genotype to rule out any changes in general androgen levels, which may explain any potential behavioral differences ((Zuloaga et al., 2007)). We found no significant differences when the seminal vesicle weights were normalized to the total body weight of each mouse (Figure 3E). Taken together, these data suggest re-expression of AP-2ε in KO mice can re-establish the functional properties of basal VSNs.

Ectopic expression of AP-2ε in mature apical VSNs increases the expression of basal specific markers leading to a progressive disorganization of the VNE.

Several AP-2 family members have been proposed to have pioneer activity (Fernandez Garcia et al., 2019; Rothstein and Simoes-Costa, 2020; Seberg et al., 2017; Williams et al., 2009). We tested whether ectopic AP-2ε expression can induce an alternative genetic program in postmitotic neurons. Olfactory marker protein (OMP) is an accepted marker for postmitotic/maturing olfactory and vomeronasal sensory neurons (Buiakova et al., 1994; Enomoto et al., 2011; Farbman and Margolis, 1980). By analyzing our scSeq data from OMPCre$^{+/-}$ mice, we found that OMP mRNA expression in maturing apical neurons begins shortly after the apical basal dichotomy is established (Figure 1E). We concluded that OMP can serve as a suitable genetic entry-point to test whether AP-2ε can redirect apical neurons toward a basal neuron identity. Thus, we used an OMPCre mouse line to drive expression of AP-2ε (OMPCre$^{+/-}$/R26AP2$\varepsilon^{+/-}$) in all olfactory and vomeronasal neurons. In this manuscript we will often refere to OMPCre$^{+/-}$/R26AP2$\varepsilon^{+/-}$ as

ectopic mutants. Notably, both apical and basal VSNs express several known Tfap2 cofactors, including Cited2 and p300/CBP (Bamforth et al., 2001; Bragança et al., 2003; Eckert et al., 2005)(Supplementary Figure S1) suggesting that both VSN populations are molecularly competent for functional AP-2ε transcriptional activity.

Immunostaining against AP-2ε on P10 OMPCre$^{+/-}$ controls showed that AP-2ε expression was limited to basal VSNs with no AP-2ε immunoreactivity in the main olfactory epithelium (OE) (Figure 4A, Figure S2A). However, in OMPCre$^{+/-}$/R26AP2ε$^{+/-}$ mutants, we found immunodetectable AP-2ε in the main olfactory epithelium (Figure S2B) and, as expected, in both apical and basal VSNs (Figure 4E). Notably, in OMPCre$^{+/-}$ /R26AP2ε$^{+/-}$ mice, we also observed sparse AP-2ε expression in sustentacular cells lining the lumen of the VNO (Figure 4E). These results suggest that OMPCre recombination can also occur in sustentacular cells. OMPCre$^{+/-}$ controls and OMPCre$^{+/-}$/R26AP-2ε$^{+/-}$ mutants displayed comparable OE gross morphology (Supplementary Figure S2). Consistent with our observation of no ectopic V2R immunoreactivity in OE mutants (Figure S2D). However, when comparing the VNO of P10 controls and OMPCre$^{+/-}$ /R26AP2ε$^{+/-}$ mutants, we observed that OMPCre$^{+/-}$/R26AP-2ε$^{+/-}$ mice had a significantly broader expression of Gαo (Figure 4B,F) and V2R2 (Figure 4C,G), spanning from basal VNO regions to the lumen. scRNA-Seq data from OMPCre$^{+/-}$ controls and OMPCre$^{+/-}$ /R26AP2ε$^{+/-}$ confirmed that apical VSNs expressing AP-2ε had variable, but a significant ($P<0.05$) upregulation, of the basal specific markers Gαo and Vmn2r7 (Figure 4, I,J).

Analysis at P21 revealed a higher number of individual or small clusters of cells ectopically expressing basal markers in the apical regions (Figure 4O-S). In adult OMPCre$^{+/-}$/R26AP2ε$^{+/-}$ mutants, we noticed an increasing level of cellular disorganization of the VNE with: 1) VSNs spanning from basal territories to regions of the lumen devoid of Sox2+ sustentacular cells, and 2) ectopic sustentacular cells organized in spherical structures or intraepithelial cysts with a subsidiary lumen within apical and basal territories (Figure 5, B-C). Notably, the regions with ectopic sustentacular cells appeared to be mostly surrounded by apical VSNs expressing AP-2ε, Meis2, and Sox2 and were enriched in the intermediate zones of the VNE (Figure 5 B-D). Interestingly, a low level of Sox2 immunoreactivity was observed in Meis2+ VSNs in both controls and OMPCre$^{+/-}$

/R26AP2ε$^{+/-}$ mice with higher intensity in cells closer to the sustentacular cell layer (Figure S3).

The affinity and positioning of epithelial cells are largely dictated by the expression of surface adhesion molecules (Fagotto, 2014; Polanco et al., 2021). Transcriptome comparison of OMPCre$^{+/-}$/R26AP2ε$^{+/-}$ mutants and controls suggest that the aberrant cell positioning in the VNE of mutants can arise from broad variations in expression levels of multiple adhesion molecules throughout Meis2+ cells (Figure 5 E).

Furthermore, scRNA-Seq of the adult OMPCre$^{+/-}$/R26AP2ε$^{+/-}$ allowed us to understand whether sustentacular cells with ectopic AP-2ε expression were contributing to the disorganization of the VNE. By performing differential gene expression analysis on the AP-2ε positive and negative sustentacular cells from the adult OMPCre$^{+/-}$/R26AP2ε$^{+/-}$ mice we observed significantly dysregulated genes (550 upregulated; 571 downregulated, adjusted p-value<0.05) with enrichment of genes related to tight-junctions, cell-cell adhesion, and cytoskeletal organization (Figure 3C,D), which may contribute to the disorganized neuroepithelium.

AP-2ε can partially reprogram VSN neuronal identity of OMPCre$^{+/-}$ and OMPCre$^{+/-}$ /R26AP2ε$^{+/}$

To further elucidate the gene expression changes in Meis2+ VSNs after AP-2ε expression, we analyzed the UMAPs using scSeq from VSNs in controls and mutant mice. These revealed similar clustering at the stages of neurogenesis and differentiation across genotypes (Figure 6A-B). However, control animals showed AP-2ε expression was limited to maturing basal VSNs (Figure 6A'-A'''). In OMPCre$^{+/-}$/R26AP-2ε$^{+/-}$ mutants, ectopic AP-2ε mRNA was also expressed in maturing and mature apical neurons (Figure 5B', B'''). When analyzing the UMAPs, we noticed that mature apical VSNs in the controls formed a distinct and independent cluster (Figure 6A-A'''), while the apical and basal clusters appeared to converge in OMPCre$^{+/-}$/R26AP-2ε$^{+/-}$ mutants (Figure 6B-B''').

To understand the extent to which AP-2ε can reprogram apical VSNs, we compared the expression of the most enriched genes in apical and basal VSNs of OMPCre$^{+/-}$ controls to the apical VSNs of OMPCre$^{+/-}$/R26AP-2ε$^{+/-}$. Interestingly, this

analysis revealed that apical VSNs of OMPCre$^{+/-}$/R26AP-2$\varepsilon^{+/-}$ mice had a mixed apical-basal expression profile with a significant down-regulation of ~22% of the apical-enriched genes (7/32), and a significant upregulation of ~28% of the basal-enriched genes (20/71) (Figure 6 C; Supplementary Table S2). Of the aberrantly expressed genes in the apical VSNs of OMPCre$^{+/-}$/R26AP-2$\varepsilon^{+/-}$ mice, we identified a reduction in Calreticulin (Calr) mRNA levels together with a strong upregulation of Calreticulin4 (Calr4), which persists in adulthood (Figure 6 D-G, Table S2, Figure S6 A,C)(Dey and Matsunami, 2011). ISH at P11 confirmed that Calr4 is normally expressed by basal VSNs in controls. However, in OMPCre$^{+/-}$/R26AP2$\varepsilon^{+/-}$ mutants Calr4 mRNA was found in both apical and basal VSNs (Figure 6D-I). In line with previous studies (Dey and Matsunami, 2011), we found that Calr was expressed below ISH detectability.

Axonal projection along the anterior posterior axis of the AOB is determined by axon guidance molecules such as Nrp2, Robo2 while the the coalescence of vomeronasal sensory neuron axons into glomeruli is largely dictated by Kirrel adhesion molecules(Cloutier et al., 2002; Prince et al., 2013; Prince et al., 2009; Vaddadi et al., 2019). Notably, the mRNA expression levels for the guidance receptors, Robo2 and Nrp2, and the adhesion molecules, Kirrel2 and Kirrel3, did not significantly change after ectopic AP-2ε expression. In fact, by immunostaining against Robo2 and Nrp2 we confirmed immunoreactivity of Nrp2 in the anterior and Robo2 in the pAOB similar to controls and observed no significant differences in the average size of anterior or posterior AOB between genotypes (Figure S4 A,B,E). Moreover, quantifications based on Kirrel2 and Kirrel3 immunostaining did not reveal major changes in glomerular size or number in the AOB (Figure S4 C,D,F,G)(Bahreini Jangjoo et al., 2021).

Single cell transcriptome analysis of apical and basal neurons of WT controls and OMPCre$^{+/-}$/R26AP2$\varepsilon^{+/-}$mutants at P60 highlighted perduring ectopic expression of basal specific genes in apical neurons and downregulation in the expression of apical specific markers including Meis2 (Supplementary Fig S6A,C). At this stage, we observed some aberrant gene expression in the basal OMPCre$^{+/-}$/R26AP-2$\varepsilon^{+/-}$ neurons compared to OMPCre$^{+/-}$/R26AP-2$\varepsilon^{+/-}$ controls (Figure S6B). These data suggest that AP-2ε can partially reprogram postnatal apical neurons. This prolonged AP-2ε overexpression may trigger a dose dependent effect in gene expression. These data suggest that AP-

2ε expression in maturing/mature VSNs is sufficient to upregulate portions of the basal VSN genetic program and repress a portion of the apical VSN genetic program bypassing cellular plasticity restrictions.

Identification of direct AP-2ε targets via CUT&RUN

Our findings suggest a key role for AP-2ε in controlling the expression of specific basal specific genes. Transcriptomic studies in AP-2ε^{Null} mice showed loss of expression of basal VSN specific genes suggesting that AP-2ε controls parts of the basal and apical VSN genetic programs (Lin et al., 2018). However, it remains unknown whether AP-2ε regulates VSN genetic programs directly or indirectly. So, we performed genome-wide mapping of transcription factor occupancy with cleavage under targets and release using nuclease (CUT&RUN) to determine the direct genetic targets of AP-2ε in the VNO to pair with our scRNA-Seq (Figure 6J-M). Our analyses identified over 3000 replicable peaks in VNO tissue indicating AP-2ε binding sites (Figure 6J). Of these putative binding sites, we found that 59.1% of the peaks occurred in promoter regions (defined as any region 1000bp upstream or 200bp downstream a transcription start site), 19.54% in distal intergenic regions, and ~17.78% in intronic regions (Figure 6H). These results suggest that most AP-2ε activity directly regulates transcription, with perhaps a secondary role in enhancer regions.

When we compared AP-2ε direct targets with our identified apical and basal enriched genes from mature VSN populations, we discovered that 15.6% of our identified apical-enriched genes (5/32 genes) (Supplementary Table 1) were AP-2ε direct targets and approximately 27% of our identified basal-enriched genes (21/71 genes) are AP-2ε direct targets (Figure 6H). Of the canonical apical and basal markers and signal transduction machinery only Gαi2/Gnai2 had putative direct AP-2ε occupancy and assumed regulation of transcription (Figure S5C). Notably, our newly discovered list of basal enriched genes (Supplementary Table 1) indicated that only Krt18 showed a putative AP-2ε binding site within its promoter region. As expected from a terminal selector gene, these data suggest that AP-2ε directly binds and regulates batteries of apical and basal enriched genes (Figure S5C).

After ectopic AP-2ε expression, only a portion of the apical and basal enriched genes were significantly up/down-regulated. When we compared the AP-2ε direct targets with the statistically significant upregulated and down-regulated genes in the OMPCre$^{+/-}$/R26AP-2ε$^{+/-}$ mutants, we observed that AP-2ε had direct control over several downregulated and upregulated genes (Supplementary Figure S4). These data suggest that AP-2ε plays a dual role in maintaining the basal VSNs' genetic program while restricting the expression of genes normally enriched in apical VSNs (Supplementary Fig S5).

Gene Ontology analysis of genes associated with AP-2ε peaks showed an enrichment of factors involved in protein degradation, transcription coregulator activity, and histone and chromatin modification (Supplementary Figure S5A). Motif enrichment analysis of AP-2ε peaks revealed Tfap2 as the top enriched motif (p=1e-180), as expected. Other transcription factor motifs enriched in the same regions as AP-2ε peaks include SP, KLF, EBF, RFX, NRF, DLX, and LHX transcription factor families (Supplementary Fig S4B). As many transcription factors work with other cofactors to regulate gene expression (Huang et al., 2015; Monahan et al., 2017), these motifs may represent potential cofactors that work in concert with AP-2ε to mediate either an activating or repressive role in the VNO.

Ectopic AP-2ε does not alter socio-sexual behaviors

To determine whether the aberrant gene expression in apical VSNs could alter VSNs' functions and related social behaviors, we evaluated intermale aggression and odorant preference (Koolhaas et al., 2013). By performing resident intruder tests, we showed that the level of intermale aggression of OMPCre$^{+/-}$/R26AP-2ε$^{+/-}$ male mice trended higher but not significantly different than WT controls (Figure 7G). However, among the animals that displayed aggressive behavior we observed significant increase in the number of attacks from WT to OMPCre$^{+/-}$/R26AP-2ε$^{+/-}$ mutants (p=0.0015; WT=16.00 SE+/- 3.1; Ectopic=43.75 SE+/- 4.8). The odorant preference test in male mice also revealed that OMPCre$^{+/-}$/R26AP-2ε$^{+/-}$ mutants exhibited preferential interest in whole female urine similar to controls (Figure 7H). All together these data suggest that ectopic

AP-2ε expression does not disrupt intermale aggression behavior nor sex odorants discrimination in males (Figure 7H). When we tested OMPCre$^{+/-}$/R26AP-2ε$^{+/-}$ females, we observed much more variability in their individual odor preferences compared to controls, even though still retained their preference for opposite sex odorants. These data indicate that ectopic AP-2ε expression in apical VSNs does not dramatically impair sex odorants discrimination.

Reduced apical VSNs' activation in response to female specific odorants

Whole male mouse urine activates both V1Rs and V2Rs (Krieger et al., 1999), while female odorants preferentially activate apical VSNs (Dudley and Moss, 1999; Norlin et al., 2001; Silvotti et al., 2018). To determine if OMPCre$^{+/-}$/R26AP-2ε$^{+/-}$ mice had altered chemodetection we quantified VSNs' activation after exposure to either male or female soiled bedding. After exposure to the soiled bedding, brains were collected after 90 minutes to allow adequate time for the phosphorylation of the ribosomal protein S6 (pS6) in the VSNs' cell bodies (Silvotti et al., 2018). VSNs activation was quantified after immunostaining against pS6 (Ser 240/244) on coronal sections of the VNO (Figure 6A-D). Apical and basal neurons were identified with Meis2 immunostaining against Meis2 and categorized as either pS6+/Meis2+ apical or pS6+/Meis2- basal VSNs (Figure 6A-D). We found that male OMPCre$^{+/-}$/R26AP-2ε$^{+/-}$ mutants had similar patterns of activation to WT controls (Figure 6A,B,E). Notably, we observed a slight but non-significant increase in the number of activated basal VSNs OMPCre$^{+/-}$/R26AP-2ε$^{+/-}$ (Figure 6E). These data suggest that ectopic expression of AP-2ε may enhance the ability of basal VSNs to detect male-specific odorants or the number neurons with basal features.

When we exposed OMPCre$^{+/-}$/R26AP-2ε$^{+/-}$ mutants to female odorants, we found an expected selective activation of apical VSNs in WT mice (Silvotti et al., 2018)(Figure 7E,F,H). Notably, fewer VSNs from female OMPCreR26AP-2ε mutants were activated than controls when female were exposed to female soiled bedding (Figure 7H). Further analysis showed that while no significant difference in the number of basal VSNs were activated between WT and mutants, there was a dramatic decrease in the number of apical VSNs activated by the female bedding (Figure 7H). These data indicate, as

observed after conditional Gαi2 ablation (Trouillet et al., 2019), that LOF of apical VSNs does not translate in major behavioral changes.

Interestingly, we also observed that OMPCre$^{+/-}$/R26AP-2ε$^{+/-}$ mutants had pS6 immunoreactivity in some sustentacular cells after exposure to male and female soiled bedding that was not present in WT controls (Figure 7E,F). We found no indications that the sustentacular cells gained the ability to detect chemosignals when we did the differential gene expression analysis of sustentacular cells of WT and mutants as we found no significant upregulation of V1R/V2R signal transduction machinery (Gnao1, Gnai2, V1Rs, V2Rs, Trpc2.. Intriguingly, we observed a decrease in genes involved in dephosphorylation (i.e. Ppp1r15a, Ppp2ca, Figure S3) in the mutant sustentacular cells, suggesting that a decrease in phosphatase activity may lead to the sustained phosphorylation of Rps6.

DISCUSSION

Understanding how differentiated neurons retain cellular plasticity remains critical to identify how genetic insults can compromise neuronal identity, circuit assembly and function (Hobert and Kratsios, 2019; Molyneaux et al., 2007; Patel and Hobert, 2017; Pereira et al., 2019; Rahe and Hobert, 2019). Spatial and temporal expression of terminal selector genes regulates the establishment and maintenance of neuronal identity remains foundational to elucidate the assembly of functional neuronal circuits (Arlotta et al., 2005; Cau et al., 2002; Cau et al., 1997; Molyneaux et al., 2007). In fact, loss of terminal selector genes can lead to loss of neuronal identity and increase cellular/phenotypic plasticity, while expression of specific TFs can induce specific cellular features only at particular developmental windows (Hobert, 2008; Rahe and Hobert, 2019).

Rodents and some marsupials have a binary vomeronasal epithelium where the two main types of VSNs, apical and basal VSNs, are generated throughout life from a common pool of Ascl1 progenitors (Berghard and Buck, 1996; Jia and Halpern, 1996; Katreddi and Forni, 2021; Mohrhardt et al., 2018; Silva and Antunes, 2017; Taroc et al., 2020; Weiler et al., 1999). The generation of these two distinct populations is central for critical socio-sexual behavior in rodents (Oboti et al., 2014; Perez-Gomez et al., 2014). In this study, we used the mouse VNO as a model system and combined scRNA-Seq,

histology, behavior, and CUT&RUN methodologies to show that the TF AP-2ε is a basal VSN specific terminal selector gene capable of partially reprogramming the apical VSN identity.

Using scRNA-Seq, we discovered key transcriptomic differences between mature basal and apical VSNs that were previously unreported (Figure 1J, Supplementary Table S1). We also demonstrated that AP-2ε mRNA is restricted to maturing Gαo/basal VSNs (Figure 1G) and that AP-2ε itself does not initiate the basal VSN differentiation program, but rather maintains the integrity of the basal neuronal identity. We discovered that AP-2ε is indispensable for normal territorial and sex-preference behaviors by reestablishing AP-2ε expression in AP-2ε KOs. We also elucidated that it acts in controlling VSN gene expression through activating and repressive activity when analyzing mature/maturing Meis2+ apical VSNs in OMPCre$^{+/-}$/R26AP-2ε$^{+/-}$ mutant mice.

During differentiation chromatin barriers dynamically restrict the cellular plasticity that prevents ectopic terminal selector genes from genetically reassigning neurons (Rahe and Hobert, 2019). We previously demonstrated in AP-2ε KOs that postmitotic VSNs can deviate from the basal differentiation program and turn on sets of apical specific genes, but AP-2ε LOF did not prevent basal neurons from acquiring basal features, such as Gαo or V2Rs (Lin et al., 2018). These data suggested that AP-2ε activity is crucial to restrict basal VSN phenotypic plasticity (Lin et al., 2018). Here we showed that AP-2ε null mice display reduced odorant sex preference and intermale aggressive behavior, which are classic phenotypes related to basal VSN LOF (Stowers et al., 2002). However, we found that reintroducing AP-2ε in maturing basal AP-2ε KO neurons was sufficient to rescue cellular homeostasis, physiological functions, and related behavior.

Terminal selectors define neuronal identity by suppressing alternative programs and can also act as pioneer factors (Lupien et al., 2008; Magnani et al., 2011; Mangale et al., 2008). Based on our data, we conclude that AP-2ε can partially reprogram the transcriptome of differentiated cells, as expected from a pioneer factor and other members of the Tfap2 family (Rothstein and Simoes-Costa, 2020). When we used OMPCre drivers to induce ectopic AP-2ε in differentiated olfactory and vomeronasal neurons, we observed progressive gene and morphological changes in the VNO, but no

gross morphological changes in the main olfactory epithelium. We suspect the lack of phenotype in the OE may arise from the absence of necessary Tfap2 cofactors , that are expressed in the VNO (Figure S1, (Eckert et al., 2005)).

The co-expression of AP-2ε in Meis2+ apical VSNs in OMPCre$^{+/-}$/R26AP-2ε$^{+/-}$ mice revealed that Meis2 and most apical specific genes showed comparable expression levels between controls and mutant animals at P10 (Figure 5A-B). However, single-cell transcriptome analyses in adult mice indicated that several apical genes including Meis2, were expressed at significantly lower levels than controls (Figure S6 A,C). These data suggest that AP-2ε acts as a terminal selector protein that negatively affects a portion of the apical program.

Ectopic expression of individual terminal selector genes selectively can control specific molecular features linked to neuronal function and identity, but not pan-neuronal features like guidance cue receptors (Patel and Hobert, 2017; Stefanakis et al., 2015). Single-cell RNA-Seq revealed that AP-2ε ectopic expression, surprisingly, does not alter the expression of VSN-specific guidance cue receptors Nrp2 and Robo2 (Cho et al., 2011; Prince et al., 2009; Walz et al., 2002) (Cloutier et al., 2002). Changes in Kirrel2 and Kirrel3 expression were not statistically significant. In accord with this, we did not find obvious changes in glomeruli size or number in the AOB (Figure S4 C,D,F,G).

In OMPCre$^{+/-}$/R26AP-2ε$^{+/-}$ mutants, we observed that the cellular organization and lamination of the vomeronasal epithelium became severely disrupted between P10 and adult ages. Notably, we found in mutants basal neurons located at the level of the VNE lumen and ectopic sustentacular cells forming intraepithelial cyst-like structures in both apical and basal territories (Figure 5B,C). Notably, the disorganization of the VNE that resembles intraepithelial cysts as previously described in aging mice (Wilson and Raisman, 1980), appeared to be more pronounced/frequent in regions proximal to the neurogenic marginal zones (Figure 5D,E), where OMP mRNA is expressed following Gap43 expression. Therefore, we posit that the regionalization of the VNE phenotypes might represent cells that underwent AP-2ε ectopic expression at early maturation stages. When we compared mRNA of control and ectopic AP-2ε mutants, which have disorganized VNE, we observed changes in expression levels of many surface and cell adhesion related molecules as well as upregulation of stress related genes (Figure 5F,

S3E). In addition to this, scRNA-seq analysis of AP-2ε positive and negative sustentacular cells in adult OMPCre$^{+/-}$/R26AP-2ε$^{+/-}$ mutants revealed massive changes in gene expression in these support cells. Future studies should focus on understanding which of the dysregulated genes in VSNs and sustentacular cells contribute to the cytoarchitectural organization of VSNs and sustentacular cells.

To elucidate the mechanism of action of AP-2ε, we performed CUT&RUN (Skene et al., 2018; Skene and Henikoff, 2017). This analysis identified putative direct targets of AP-2ε and showed 3000+ putative binding sites in the vomeronasal tissue. Of these, we found that most of binding sites were primarily in promoter regions, not in intergenic and intronic regions. These data suggest that AP-2ε's main mechanism of action directly regulates gene transcription with perhaps a secondary role at enhancer regions. We found AP-2ε bound to the up and down-regulated genes in both apical VSNs and sustentacular cells in the OMPCre$^{+/-}$/R26AP-2ε$^{+/-}$ ectopic mouse line, which suggests that AP-2ε can act as both a transcriptional activator and repressor. Motif analysis of these up and downregulated regions indicates that AP-2ε may function in concert with specific transcriptional cofactors to fulfill a dual role in maintaining the basal VSN genetic program and restricting cellular plasticity. Notably our CUT&RUN data showed an enrichment of factors involved in transcription coregulator activity, histone modification, and chromatin modification (Figure S5 A). These data suggest that AP-2ε may play a role in modifying the chromatin landscape indirectly or in tandem with these transcriptional cofactors to regulate the basal genetic program. Even though transcriptome and histological analysis of the VNE showed significant changes in canonical apical and basal specific genes, only Gαi2 and Krt18 had AP-2ε peak assignments, suggesting that AP-2ε acts indirectly to regulate these genes. However, since peaks were assigned to the nearest gene, we cannot exclude long-distance gene regulation through enhancer regions as a contributor.

Sex odorants activate different sets of vomeronasal receptors and therefore different populations of VSNs (Dudley and Moss, 1999; Keller et al., 2006; Silvotti et al., 2018). Interestingly, scRNA-seq analysis and validation via ISH revealed that ectopic AP-2ε in mature apical VSNs had upregulated Calreticulin-4 (Calr4) ER chaperone proteins, which has been previously shown to increase V2R cell surface expression (Dey and

Matsunami, 2011). These data suggest that ectopic AP-2ε in mature apical VSNs may indirectly disturb vomeronasal receptor expression or insertion and therefore alter the ability of VSNs to detect and process sex-specific odorants.

Using pS6 immunoreactivity on activated VSNs after male odorant exposure indicated a potential sensitization of basal VSNs and unchanged activation of apical VSNs after ectopic AP-2ε expression. Conditional ablation of normal apical VSN signal transduction does not undermine intermale aggression, rather it enhances territorial aggression in mutant males (Trouillet et al., 2019). In line with this, we found that OMPCre$^{+/-}$/R26AP-2ε$^{+/-}$ mutants that display aggressive behavior had higher levels of aggression towards male intruders when compared to WT controls. However, the nonsignificant changes in pS6 activation after male odorant exposure suggest that the LOF in apical VSNs might occur in processing or signaling rather than detection of stimuli. These data indicate that ectopic AP-2ε expression is sufficient to subvert the function of apical VSNs and therefore alter intrinsic social behaviors.

Strikingly, female OMPCre$^{+/-}$/R26AP-2ε$^{+/-}$ showed significantly decreased activation of apical VSNs in response to female bedding compared to controls. In rodents, olfactory sex discrimination persists after VNO excision; however, preference for opposite sex odorants is mediated by the accessory olfactory system (Keller et al., 2006; Pankevich et al., 2004). Despite the putative desensitization of the apical VSNs in OMPCre$^{+/-}$/R26AP-2ε$^{+/-}$ mutants, transcriptome and morphological changes in the VNO did not compromise normal sex odorant preference in male or female mutants. In fact, conditional ablation of Gαi2, which is required for normal signaling of apical VSNs, did not alter normal male sexual behavior, including male preference for estrous female urine (Trouillet et al., 2019). Together, these data indicate that though ectopic AP-2ε expression in apical VSNs subverts the function of apical VSNs it does not alter normal sex identification and territorial behaviors (Trouillet et al., 2019) , confirming a dispensable role for these neurons in the tested behaviors.

In conclusion, the results of our study indicate that AP-2ε has many features of a terminal selector gene with roles in controlling the expression of several basal VSN genes and repressing apical ones, which is necessary for normal basal VSN functions that mediate territorial and sex preference behaviors in mice. We showed that AP-2ε has an

548 extraordinary ability in reprogramming the transcriptome of postnatal VSNs in rodents and
549 confers an ambiguous transcriptome identity to these cells bypassing cellular plasticity
550 restrictions over time.

551 Our study suggests that as previously hypothesized by others (Hobert and
552 Kratsios, 2019; Rahe and Hobert, 2019) aberrant expression of terminal selector genes
553 in postnatal cells can alter the organization of a neuroepithelium, the transcriptomic
554 identity of neurons and lead to neuronal pathologies.

555

556 **ACKNOWLEDGEMENTS**

557 ***Funding***

558 This publication was supported by the National Institutes of Health (NIH) by the
559 Eunice Kennedy Shriver National Institute of Child Health and Human Development of
560 the National Institutes of Health under the Awards R15-HD096411 (P.E.F) and R01-
561 HD097331/HD/NICHD (P.E.F), the National Institute of Deafness and Other
562 Communication Disorders of the National Institutes of Health under the Award R01-
563 DC017149 (P.E.F), the National Institute of Dental and Craniofacial Research under the
564 Award R01DE028576 (M.S.-C), and the National Institute of Mental Health under the
565 Award R15-MH118692 (D.G.Z).

566

567 **STAR★METHODS**

568

569 **KEY RESOUCES TABLE**

570

571

572 **RESOURCE AVAILABILITY**

573

574 ***Lead contact***

575 Further information and requests for resources and reagents should be directed to
576 and will be fulfilled by the lead contact, Paolo E. Forni (pforni@albany.edu).

577

578 ***Materials availability***

Mouse lines generated in this study will be deposited to Jackson Labs by the time of publication.

There are restrictions in availability of the antibody Rabbit anti-V2R2 which was obtained from the lab of Roberto Tirindelli (University of Parma, Italy) and is not commercially available.

Data and code availability

The Single-cell RNA-sequencing and CUT& RUN sequencing data discussed in this publication have been deposited at NCBI's Gene Expression Omnibus and are publicly available as of the date of publication. Accession numbers are listed in the key resources table. This paper reports no original code. Any additional information required to reanalyzed the data reported in this paper is available from the lead contact upon request.

EXPERIMENTAL MODEL AND SUBJECT DETAILS

Animals

The R26AP2ε mice were produced by Cyagen (Santa Clara, CA). on a C57B/6 background. The AP-2εCre line (*Tfap2e*$^{tm1(cre)Will}$) was obtained from Dr. Trevor Williams, Department of Craniofacial Biology, University of Colorado. The R26AP-2ε (B6.Cg-Gt(ROSA)26Sor$^{tm(CAG-mTfap2e)For}$) mouse line was produced through Cyagen on a C56BL/6 background. The OMPCre line (B6;129P2-*Omp*$^{tm4(cre)Mom}$/MomJ) was obtained from Dr. Paul Feinstein (Hunter College, City University of New York) on a 129P2/OlaHsd background and backcrossed to a C57BL/6 background for 6 generations at the time of this study. The characterization and comparison of the rescue of the AP-2ε phenotype (AP-2εCreR26AP-2ε), AP-2ε KO, and wild-types were performed on a C57BL/6 background. OMPCre$^{+/-}$/R26AP2ε$^{+/-}$ mutant mice are viable. Genotyping of mutants was performed by PCR. Primers used are detailed in the Key Resources Table.

Mice were housed under a 12hr day/night cycle. Animals were collected/analyzed at P10, P21, and Adult (P60-P90) ages. For all morphological analyses both males and females were included unless otherwise specified. All mouse studies were approved

by the University at Albany Institutional Animal Care and Use Committee (IACUC). Mouse lines generated in this study will be deposited to Jackson Labs by the time of publication.

METHOD DETAILS

Generation of the AP-2ε conditional Knock-In Model

The AP-2ε conditional Knock-In allele was generated by targeting the ROSA26 gene in C57BL/6 ES cells. The "CAG-loxP-stop-loxP-mouse Tfap2e CDS-polyA" cassette was cloned into intron 1 of ROSA26 in the reverse orientation. In the targeting vector, the positive selection marker (Neo) was flanked by SDA (self-deletion anchor) site, and DTA was used for negative selection. Mouse genomic fragments containing homology arms (Has) were amplified from BAC clone by using high fidelity Taq DNA polymerase and were sequentially assembled into a targeting vector together with recombination sites and selection markers.

The ROSA26 targeting construct was linearized by restriction digestion with AscI followed by phenol/chloroform extraction and ethanol precipitation. The linearized vector was transfected into C57BL/6 ES cells according to Taconic-Cyagen's standard electroporation procedures and G418 resistant clones were selected for 24 hours post-electroporation. These were then screened for homologous recombination by PCR and characterized by Southern Blot analysis. Two separate clones, A2 and H2, were successfully transmitted to germline and characterized.

Genotyping for the R26AP-2ε mouse line was performed by PCR using R26-AP-2e Common (5' GGAGGGGGGCTCTGAGAT 3'), R26-AP-2e Mutant (5' GGCTGGTGTGGCCAATGC 3'), R26-AP-2e WT (5' GTCGTGAGGCTGCAGGTC 3') with expected bands at 552bp (Mutant) and 400bp (WT).

Resident Intruder Test

The resident intruder assay was used to evaluate aggression in male mice of mutants and controls. Test subjects were housed with intact females for at least one week prior to testing. On the day of testing, all subjects (residents and intruders) were acclimated to the experimental environment for at least 30 minutes prior to the assay. Females were removed immediately before testing. Castrated C57B mice were swabbed

with male whole urine immediately before being introduced into the resident male's home cage. Interactions between isolated residents and intruders were recorded for 10min and videos were evaluated using ButtonBox v.5.0 (Behavioral Research Solutions, Madison WI, USA) software for the number and duration of attacks.

Innate olfactory preference test

Adult mice were isolated for at least one week prior to testing. Individual mice were habituated to the experimental environment for at least 30 minutes, then to the test cage for an additional 2 minutes. After the habituation period, cotton swabs scented with either male or female whole urine was placed on either side of the test cage. The time spent sniffing each odorant was normalized to total investigation time.

Neuronal activation in response to sex-specific odorants

Adult mice were isolated for at least one week prior to exposure to either soiled bedding from male or female mice for ~90min then perfused with PBS and 3.7% formaldehyde in PBS, then collected to evaluate neuronal activation with immunohistochemistry against pS6.

Tissue Preparation

Tissue collected at ages ≥P10 were perfused with PBS then 3.7% formaldehyde in PBS. Brain tissue was isolated at the time of perfusion and then immersion-fixed for 3-4 hours at 4°C. Noses were immersion fixed in 3.7% formaldehyde in PBS at 4°C overnight and then decalcified in 500mM EDTA for 3-4 days. All samples were cryoprotected in 30% sucrose in PBS overnight at 4°C, followed by embedding in Tissue-Tek O.C.T. Compound (Sakura Finetek USA, Inc., Torrance CA) using dry ice, and stored at -80°C. Tissue was cryosectioned using a CM3050S Leica cryostat at 16μm for VNOs and 20μm for brain tissue and collected on VWR Superfrost Plus Micro Slides (Radnor, PA) for immunostaining and in situ hybridization (ISH). All slides were stored at -80°C until ready for staining.

Immunohistochemistry

For immunohistochemistry and immunofluorescence antigen retrieval was performed on slides that were submerged in citrate buffer (pH 6.0) above 95°C for at least 15min before cooling to room temperature, then permeabilized with and blocked in horse serum based blocking solution before transferring into primary antibodies overnight at 4°C. For immunohistochemistry slides were additionally incubated in an H_2O_2 solution (35mL PBS+ 15mL 100% Methanol + 500µL 30% H_2O_2) after antigen retrieval.

For chromogen-based reactions, staining was visualized with the Vectastain ABC Kit (Vector, Burlingame, CA) using diaminobenzidine (DAB) (Forni et al., 2011); sections were counterstained with methyl green and mounted with Sub-X mounting medium. For immunofluorescence species-appropriate secondary antibodies conjugated with either Alexa Fluor 488, Alexa Fluor 594, Alexa Fluor 568, Alexa Fluor 680 were used for immunofluorescence detection (Molecular Probes and Jackson ImmunoResearch Laboratories, Inc., Westgrove, PA). Sections were counterstained with 4',6'-diamidino-2-phenylindole (DAPI) (1:3000; Sigma-Aldrich), and coverslips were mounted with FluoroGel (Electron Microscopy Services, Hatfield, PA).

Confocal microscopy pictures were taken on a Zeiss LSM 710 microscope. Epifluorescence pictures were taken on a Leica DM4000 B LED fluorescence microscope equipped with a Leica DFC310 FX camera. Images were further analyzed using FIJI/ImageJ software. Antibodies and concentrations used in this study are detailed in the Key Resources Table.

In Situ Hybridization

Digoxigenin-labeled RNA probes were prepared by *in vitro* transcription (DIG RNA labeling kit; Roche Diagnostics, Basel, Switzerland). In situ hybridizations were performed on 16µm cryosections that were rehydrated in 1x PBS for 5min, fixed in 4% PFA in 0.1M phosphate buffer for 20min at 4°C, treated with 10µg/mL proteinase K (Roche) for 12min at 37°C, and then refixed in 4% PFA at 4°C for 20min. To inactivate the internal alkaline phosphatase, the tissue was treated with 0.2M HCl for 30min. Nonspecific binding of the probe to slides was reduced by dipping slides in 0.1M triethanolamine (pH 8.0)/0.25% acetic anhydride solution, then washed with 2x Saline-Sodium Citrate (SSC) buffer before incubating in hybridization solution for 2hrs at room temperature. Slides were then

hybridized with 200μl of probe in hybridization solution at 65°C overnight in a moisture chamber. After hybridization, the slides were washed in 2x SSC, briefly, then in 1x SSC/50% formamide for 40min at 65°C. RNase A treatment (10μg/mL) was carried out at 37°C for 30min. The slides were then washed with 2x SSC then 0.2x SSC for 15min each at 65°C. Hybridization was visualized by immunostaining with an alkaline phosphatase conjugated anti-DIG (1:1000), and NBT/BCIP developer solution (Roche Diagnostics). After color reaction, the slides were put into 10mM Tris-HCl pH 8.0/1mM EDTA, rinsed in PBS and air dried before mounting with Sub-X mounting medium.

Single-Cell RNA Sequencing

The vomeronasal organs of OMPCre$^{+/-}$ at P10 and OMPCre$^{+/-}$/R26AP2ε$^{+/-}$ at P10 and 3mo were isolated and dissociated into single-cell suspension using neural isolation enzyme/papain (NIE/Papain in Neurobasal Medium with 0.5mg/mL Collagenase A, 1.5mM L-cysteine and 100U/mL DNAse I) incubated at 37ºC. The dissociated cells were then washed with HBSS and reconstituted in cell freezing medium (90% FBS, 10% DMSO). Cells were frozen from room temperature to -80ºC at a -1°C/min freeze rate. Single cell suspension was sent to SingulOmics for high-throughput single-cell gene expression profiling using the 10x Genomics Chromium Platform. Data were analyzed along with using Seurat 4.0.5. The scRNA-seq data discussed in this publication have been deposited in NCBI's Gene Expression Omnibus and are accessible through GEO series accession number GSE192746 (https://www.ncbi.nlm.nih.gov/geo/query/acc.cgi?acc=GSE192746). We also utilized previously published data from (Katreddi et al., 2021), available through GEO series accession number GSE190330 (https://www.ncbi.nlm.nih.gov/geo/query/acc.cgi?acc=GSE190330).

CUT&RUN

Cells frozen in 90% FBS/10%DMSO were thawed at 37°C and resuspended in CUT&RUN wash buffer (20mM HEPES pH7.5, 150mM NaCl, 0.5mM spermidine, plus Roche Complete Protease inhibitor, EDTA-free). CUT&RUN experiments were performed as previously described (Meers et al., 2019) with minor modifications. 0.025%

734 digitonin was used for the Dig-wash buffer formulation. Antibody incubation was
735 performed overnight at 4°C, followed by Protein A-MNase binding for 1 hour at 4°C. Prior
736 to targeted digestion, cell-bead complexes were washed in low-salt rinse buffer (20mM
737 HEPES pH7.5, 0.5mM spermidine, 0.025% digitonin, plus Roche Complete Protease
738 inhibitor, EDTA-free) followed by targeted digestion in ice-cold high-calcium incubation
739 buffer (3.5 mM HEPES pH 7.5, 10 mM $CaCl_2$, 0.025% Digitonin) for 30 minutes at 0°C.
740 Targeted digestion was halted by replacing the incubation buffer with EGTA-STOP buffer
741 (170 mM NaCl, 20 mM EGTA, 0.025% digitonin, 20 µg/ml glycogen, 25 µg/ml RNase A),
742 followed by chromatin release and DNA extraction. Protein AG–MNase was kindly
743 provided by Dr. Steve Henikoff. A rabbit polyclonal Anti-TFAP2E antibody (Proteintech
744 25829-1-AP) was used at a concentration of 1:50 for CUT&RUN experiments.
745
746 ***CUT&RUN library preparation***
747 CUT&RUN libraries were prepared using the NEBNext ultra II DNA library prep kit (New
748 England Biolabs E7645). Quality control of prepared libraries was conducted using an
749 ABI 3730xl DNA analyzer for fragment analysis. Libraries were pooled to equimolar
750 concentrations and sequenced with paired-end 37-bp reads on an Illumina NextSeq 500
751 instrument.
752
753 **QUANTIFICATION AND STATISTICAL ANALYSIS**
754
755 ***Quantification and statistical analyses of microscopy data.***
756 All data were collected from mice kept under similar housing conditions in transparent
757 cages on a normal 12 hr. light/dark cycle. Tissue collected from either males or females
758 in the same genotype/treatment group were analyzed together unless otherwise stated.
759 Ages analyzed are indicated in text and figures. The data are presented as mean ± SEM.
760 Prism 9.2.0 was used for statistical analyses, including calculation of mean values, and
761 standard errors. Two-tailed, unpaired t-test were used for all statistical analyses, and
762 calculated p-values <0.05 were considered statistically significant. Sample sizes and p-
763 values are indicated as single points in each graph and/or in figure legends.

Measurements of VNE and cell counts were performed on confocal images or bright field images of coronal serial sections immunostained or in situ hybridizations for the indicated targets. In animals ≥P15, the most central 6-8 sections on the rostro-caudal axis of the VNO were quantified and averaged, and in animals ≥P0, the most medial 4-6 sections were quantified and averaged. Measurements and quantifications were performed using ImageJ 2.1.0 and Imaris. Statistical differences between genotypes were quantified with two-tailed unpaired t-test using Prism 9.2.0, (GraphPad Software, CA, USA). Microscopy data reported in this paper will be shared by the lead contact upon request.

CUT&RUN data analysis

In processing CUT&RUN data, paired-end sequencing reads were trimmed using Cutadapt t(Martin, 2011) using the following arguments: "-a AGATCGGAAGAGCACACGTCTGAACTCCAGTCA -A AGATCGGAAGAGCGTCGTGTAGGGAAAGAGTGT --minimum-length=25". Reads were aligned to the reference mouse mm10 assembly from the UCSC genome browser using Bowtie 2 (Langmead and Salzberg, 2012) using the following arguments: "--local --very-sensitive-local --no-unal --no-mixed --no-discordant -I 10 -X 1000". BAM files were filtered with SAMtools to discard unmapped reads, those which were not the primary alignment, reads failing platform/vendor quality checks, and PCR/optical duplicates (-f 2 -F 780). Peak calling was performed using MACS2 (Zhang et al., 2008). Peak-gene annotation was done by mapping peaks to their closest annotated gene using the ChIPseeker R package(Yu et al., 2015). GO term analysis was performed in R using clusterProfiler (Yu et al., 2012). Motif enrichment analysis was performed using HOMER (Heinz et al., 2010). The data from this CUT&RUN experiment has been deposited into the NCBI's Expression Omnibus and are accessible through GEO series accession number GSE193139 (https://www.ncbi.nlm.nih.gov/geo/query/acc.cgi?acc=GSE193139).

REFERENCES

Arlotta, P., Molyneaux, B.J., Chen, J., Inoue, J., Kominami, R., and Macklis, J.D. (2005). Neuronal subtype-specific genes that control corticospinal motor neuron development in vivo. Neuron *45*, 207-221.

Bahreini Jangjoo, S., Lin, J.M., Etaati, F., Fearnley, S., Cloutier, J.-F., Khmaladze, A., and Forni, P.E. (2021). Automated quantification of vomeronasal glomeruli number, size, and color composition after immunofluorescent staining. Chemical senses.

Bamforth, S.D., Bragança, J., Eloranta, J.J., Murdoch, J.N., Marques, F.I.R., Kranc, K.R., Farza, H., Henderson, D.J., Hurst, H.C., and Bhattacharya, S. (2001). Cardiac malformations, adrenal agenesis, neural crest defects and exencephaly in mice lacking Cited2, a new Tfap2 co-activator. Nature genetics *29*, 469-474.

Bassett, E.A., Korol, A., Deschamps, P.A., Buettner, R., Wallace, V.A., Williams, T., and West-Mays, J.A. (2012). Overlapping Expression Patterns and Redundant Roles for AP-2 Transcription Factors in the Developing Mammalian Retina. Developmental dynamics : an official publication of the American Association of Anatomists *241*, 814-829.

Berghard, A., and Buck, L.B. (1996). Sensory transduction in vomeronasal neurons: evidence for G alpha o, G alpha i2, and adenylyl cyclase II as major components of a pheromone signaling cascade. The Journal of Neuroscience *16*, 909-918.

Bragança, J., Eloranta, J.J., Bamforth, S.D., Ibbitt, J.C., Hurst, H.C., and Bhattacharya, S. (2003). Physical and functional interactions among AP-2 transcription factors, p300/CREB-binding protein, and CITED2. The Journal of biological chemistry *278*, 16021-16029.

Buiakova, O.I., Krishna, N.S., Getchell, T.V., and Margolis, F.L. (1994). Human and rodent OMP genes: conservation of structural and regulatory motifs and cellular localization. Genomics *20*, 452-462.

Cau, E., Casarosa, S., and Guillemot, F. (2002). Mash1 and Ngn1 control distinct steps of determination and differentiation in the olfactory sensory neuron lineage. Development *129*, 1871-1880.

Cau, E., Gradwohl, G., Fode, C., and Guillemot, F. (1997). Mash1 activates a cascade of bHLH regulators in olfactory neuron progenitors. Development *124*, 1611-1621.

Chambers, B.E., Gerlach, G.F., Clark, E.G., Chen, K.H., Levesque, A.E., Leshchiner, I., Goessling, W., and Wingert, R.A. (2019). Tfap2a is a novel gatekeeper of nephron differentiation during kidney development. Development *146*, dev172387.

Chamero, P., Katsoulidou, V., Hendrix, P., Bufe, B., Roberts, R., Matsunami, H., Abramowitz, J., Birnbaumer, L., Zufall, F., and Leinders-Zufall, T. (2011). G protein G(alpha)o is essential for vomeronasal function and aggressive behavior in mice. Proc Natl Acad Sci U S A *108*, 12898-12903.

Chamero, P., Marton, T.F., Logan, D.W., Flanagan, K., Cruz, J.R., Saghatelian, A., Cravatt, B.F., and Stowers, L. (2007). Identification of protein pheromones that promote aggressive behaviour. Nature *450*, 899-902.

Cho, J.H., Prince, J.E., Cutforth, T., and Cloutier, J.F. (2011). The pattern of glomerular map formation defines responsiveness to aversive odorants in mice. The Journal of neuroscience : the official journal of the Society for Neuroscience *31*, 7920-7926.

Cloutier, J.F., Giger, R.J., Koentges, G., Dulac, C., Kolodkin, A.L., and Ginty, D.D. (2002). Neuropilin-2 mediates axonal fasciculation, zonal segregation, but not axonal convergence, of primary accessory olfactory neurons. Neuron *33*, 877-892.

de la Rosa-Prieto, C., Saiz-Sanchez, D., Ubeda-Banon, I., Argandona-Palacios, L., Garcia-Munozguren, S., and Martinez-Marcos, A. (2010). Neurogenesis in subclasses of vomeronasal sensory neurons in adult mice. Developmental neurobiology *70*, 961-970.

Dey, S., and Matsunami, H. (2011). Calreticulin chaperones regulate functional expression of vomeronasal type 2 pheromone receptors. Proc Natl Acad Sci U S A *108*, 16651-16656.

Dudley, C.A., and Moss, R.L. (1999). Activation of an anatomically distinct subpopulation of accessory olfactory bulb neurons by chemosensory stimulation. Neuroscience *91*, 1549-1556.

Dulac, C., and Axel, R. (1995). A novel family of genes encoding putative pheromone receptors in mammals. Cell *83*, 195-206.

Eckert, D., Buhl, S., Weber, S., Jager, R., and Schorle, H. (2005). The AP-2 family of transcription factors. Genome biology *6*, 246.

Enomoto, T., Ohmoto, M., Iwata, T., Uno, A., Saitou, M., Yamaguchi, T., Kominami, R., Matsumoto, I., and Hirota, J. (2011). Bcl11b/Ctip2 controls the differentiation of vomeronasal sensory neurons in mice. The Journal of neuroscience : the official journal of the Society for Neuroscience *31*, 10159-10173.

Fagotto, F. (2014). The cellular basis of tissue separation. Development *141*, 3303-3318.

Farbman, A.I., and Margolis, F.L. (1980). Olfactory marker protein during ontogeny: immunohistochemical localization. Dev Biol *74*, 205-215.

Feng, W., Simoes-de-Souza, F., Finger, T.E., Restrepo, D., and Williams, T. (2009). Disorganized olfactory bulb lamination in mice deficient for transcription factor AP-2epsilon. Mol Cell Neurosci *42*, 161-171.

Feng, W., and Williams, T. (2003). Cloning and characterization of the mouse AP-2 epsilon gene: a novel family member expressed in the developing olfactory bulb. Mol Cell Neurosci *24*, 460-475.

Fernandez Garcia, M., Moore, C.D., Schulz, K.N., Alberto, O., Donague, G., Harrison, M.M., Zhu, H., and Zaret, K.S. (2019). Structural Features of Transcription Factors Associating with Nucleosome Binding. Molecular cell *75*, 921-932 e926.

Forni, P.E., Fornaro, M., Guenette, S., and Wray, S. (2011). A role for FE65 in controlling GnRH-1 neurogenesis. The Journal of neuroscience : the official journal of the Society for Neuroscience *31*, 480-491.

Heinz, S., Benner, C., Spann, N., Bertolino, E., Lin, Y.C., Laslo, P., Cheng, J.X., Murre, C., Singh, H., and Glass, C.K. (2010). Simple combinations of lineage-determining transcription factors prime cis-regulatory elements required for macrophage and B cell identities. Molecular cell *38*, 576-589.

Herrada, G., and Dulac, C. (1997). A novel family of putative pheromone receptors in mammals with a topographically organized and sexually dimorphic distribution. Cell *90*, 763-773.

Hobert, O. (2008). Regulatory logic of neuronal diversity: terminal selector genes and selector motifs. Proc Natl Acad Sci U S A *105*, 20067-20071.

Hobert, O., and Kratsios, P. (2019). Neuronal identity control by terminal selectors in worms, flies, and chordates. Curr Opin Neurobiol *56*, 97-105.

Huang, Y.H., Jankowski, A., Cheah, K.S., Prabhakar, S., and Jauch, R. (2015). SOXE transcription factors form selective dimers on non-compact DNA motifs through multifaceted interactions between dimerization and high-mobility group domains. Scientific reports *5*, 10398.

Isogai, Y., Si, S., Pont-Lezica, L., Tan, T., Kapoor, V., Murthy, V.N., and Dulac, C. (2011). Molecular organization of vomeronasal chemoreception. Nature *478*, 241-245.

Jia, C., and Halpern, M. (1996). Subclasses of vomeronasal receptor neurons: differential expression of G proteins (Gi alpha 2 and G(o alpha)) and segregated projections to the accessory olfactory bulb. Brain research *719*, 117-128.

Kantarci, H., Edlund, R.K., Groves, A.K., and Riley, B.B. (2015). Tfap2a Promotes Specification and Maturation of Neurons in the Inner Ear through Modulation of Bmp, Fgf and Notch Signaling. PLoS genetics *11*, e1005037.

Katreddi, R.R., and Forni, P.E. (2021). Mechanisms underlying pre- and postnatal development of the vomeronasal organ. Cell Mol Life Sci.

Katreddi, R.R., Taroc, E.Z.M., Hicks, S.M., Lin, J.M., Liu, S., Xiang, M., and Forni, P.E. (2021). Notch signaling determines cell-fate specification of the two main types of vomeronasal neurons of rodents. bioRxiv, 2021.2010.2026.466003.

Keller, M., Pierman, S., Douhard, Q., Baum, M.J., and Bakker, J. (2006). The vomeronasal organ is required for the expression of lordosis behaviour, but not sex discrimination in female mice. The European journal of neuroscience *23*, 521-530.

Koolhaas, J.M., Coppens, C.M., de Boer, S.F., Buwalda, B., Meerlo, P., and Timmermans, P.J.A. (2013). The resident-intruder paradigm: a standardized test for aggression, violence and social stress. Journal of visualized experiments : JoVE, e4367-e4367.

Krieger, J., Schmitt, A., Lobel, D., Gudermann, T., Schultz, G., Breer, H., and Boekhoff, I. (1999). Selective activation of G protein subtypes in the vomeronasal organ upon stimulation with urine-derived compounds. The Journal of biological chemistry *274*, 4655-4662.

Langmead, B., and Salzberg, S.L. (2012). Fast gapped-read alignment with Bowtie 2. Nature methods *9*, 357-359.

Lin, J.M., Taroc, E.Z.M., Frias, J.A., Prasad, A., Catizone, A.N., Sammons, M.A., and Forni, P.E. (2018). The transcription factor Tfap2e/AP-2epsilon plays a pivotal role in maintaining the identity of basal vomeronasal sensory neurons. Dev Biol *441*, 67-82.

Luo, L., Ambrozkiewicz, M.C., Benseler, F., Chen, C., Dumontier, E., Falkner, S., Furlanis, E., Gomez, A.M., Hoshina, N., Huang, W.H.*, et al.* (2020). Optimizing Nervous System-Specific Gene Targeting with Cre Driver Lines: Prevalence of Germline Recombination and Influencing Factors. Neuron *106*, 37-65 e35.

Lupien, M., Eeckhoute, J., Meyer, C.A., Wang, Q., Zhang, Y., Li, W., Carroll, J.S., Liu, X.S., and Brown, M. (2008). FoxA1 translates epigenetic signatures into enhancer-driven lineage-specific transcription. Cell *132*, 958-970.

Magnani, L., Eeckhoute, J., and Lupien, M. (2011). Pioneer factors: directing transcriptional regulators within the chromatin environment. Trends Genet *27*, 465-474.

Mangale, V.S., Hirokawa, K.E., Satyaki, P.R., Gokulchandran, N., Chikbire, S., Subramanian, L., Shetty, A.S., Martynoga, B., Paul, J., Mai, M.V.*, et al.* (2008). Lhx2 selector activity specifies cortical identity and suppresses hippocampal organizer fate. Science *319*, 304-309.

Martin, M. (2011). Cutadapt removes adapter sequences from high-throughput sequencing reads. EMBnetjournal *17*, 10-12.

Martinez-Marcos, A., Ubeda-Banon, I., and Halpern, M. (2000). Cell turnover in the vomeronasal epithelium: evidence for differential migration and maturation of subclasses of vomeronasal neurons in the adult opossum. Journal of neurobiology *43*, 50-63.

Matsunami, H., and Buck, L.B. (1997). A multigene family encoding a diverse array of putative pheromone receptors in mammals. Cell *90*, 775-784.

Meers, M.P., Bryson, T.D., Henikoff, J.G., and Henikoff, S. (2019). Improved CUT&RUN chromatin profiling tools. Elife *8*.

Mohrhardt, J., Nagel, M., Fleck, D., Ben-Shaul, Y., and Spehr, M. (2018). Signal Detection and Coding in the Accessory Olfactory System. Chemical senses *43*, 667-695.

Molyneaux, B.J., Arlotta, P., Menezes, J.R., and Macklis, J.D. (2007). Neuronal subtype specification in the cerebral cortex. Nature reviews Neuroscience *8*, 427-437.

Mombaerts, P., Wang, F., Dulac, C., Chao, S.K., Nemes, A., Mendelsohn, M., Edmondson, J., and Axel, R. (1996). Visualizing an olfactory sensory map. Cell *87*, 675-686.

Monahan, K., Schieren, I., Cheung, J., Mumbey-Wafula, A., Monuki, E.S., and Lomvardas, S. (2017). Cooperative interactions enable singular olfactory receptor expression in mouse olfactory neurons. eLife *6*.

Montani, G., Tonelli, S., Sanghez, V., Ferrari, P.F., Palanza, P., Zimmer, A., and Tirindelli, R. (2013). Aggressive behaviour and physiological responses to pheromones are strongly impaired in mice deficient for the olfactory G-protein -subunit G8. J Physiol *591*, 3949-3962.

Murray, R.C., Navi, D., Fesenko, J., Lander, A.D., and Calof, A.L. (2003). Widespread defects in the primary olfactory pathway caused by loss of Mash1 function. The Journal of neuroscience : the official journal of the Society for Neuroscience *23*, 1769-1780.

Naik, A.S., Lin, J.M., Taroc, E.Z.M., Katreddi, R.R., Frias, J.A., Lemus, A.A., Sammons, M.A., and Forni, P.E. (2020). Smad4-dependent morphogenic signals control the maturation and axonal targeting of basal vomeronasal sensory neurons to the accessory olfactory bulb. Development *147*, dev184036.

Norlin, E.M., Alenius, M., Gussing, F., Hagglund, M., Vedin, V., and Bohm, S. (2001). Evidence for gradients of gene expression correlating with zonal topography of the olfactory sensory map. Mol Cell Neurosci *18*, 283-295.

Oboti, L., Ibarra-Soria, X., Perez-Gomez, A., Schmid, A., Pyrski, M., Paschek, N., Kircher, S., Logan, D.W., Leinders-Zufall, T., Zufall, F.*, et al.* (2015). Pregnancy and estrogen enhance neural progenitor-cell proliferation in the vomeronasal sensory epithelium. BMC Biol *13*, 104.

Oboti, L., Perez-Gomez, A., Keller, M., Jacobi, E., Birnbaumer, L., Leinders-Zufall, T., Zufall, F., and Chamero, P. (2014). A wide range of pheromone-stimulated sexual and reproductive behaviors in female mice depend on G protein Galphao. BMC Biol *12*, 31.

Pankevich, D.E., Baum, M.J., and Cherry, J.A. (2004). Olfactory sex discrimination persists, whereas the preference for urinary odorants from estrous females disappears in male mice after vomeronasal organ removal. The Journal of neuroscience : the official journal of the Society for Neuroscience *24*, 9451-9457.

Patel, T., and Hobert, O. (2017). Coordinated control of terminal differentiation and restriction of cellular plasticity. eLife *6*.

977 Patel, T., Tursun, B., Rahe, D.P., and Hobert, O. (2012). Removal of Polycomb repressive
978 complex 2 makes C. elegans germ cells susceptible to direct conversion into specific
979 somatic cell types. Cell reports *2*, 1178-1186.
980 Pellikainen, J.M., and Kosma, V.M. (2007). Activator protein-2 in carcinogenesis with a
981 special reference to breast cancer--a mini review. International journal of cancer Journal
982 international du cancer *120*, 2061-2067.
983 Pereira, L., Aeschimann, F., Wang, C., Lawson, H., Serrano-Saiz, E., Portman, D.S.,
984 Grosshans, H., and Hobert, O. (2019). Timing mechanism of sexually dimorphic nervous
985 system differentiation. eLife *8*.
986 Perez-Gomez, A., Stein, B., Leinders-Zufall, T., and Chamero, P. (2014). Signaling
987 mechanisms and behavioral function of the mouse basal vomeronasal neuroepithelium.
988 Frontiers in neuroanatomy *8*, 135.
989 Polanco, J., Reyes-Vigil, F., Weisberg, S.D., Dhimitruka, I., and Bruses, J.L. (2021).
990 Differential Spatiotemporal Expression of Type I and Type II Cadherins Associated With
991 the Segmentation of the Central Nervous System and Formation of Brain Nuclei in the
992 Developing Mouse. Front Mol Neurosci *14*, 633719.
993 Prince, J.E., Brignall, A.C., Cutforth, T., Shen, K., and Cloutier, J.F. (2013). Kirrel3 is
994 required for the coalescence of vomeronasal sensory neuron axons into glomeruli and for
995 male-male aggression. Development *140*, 2398-2408.
996 Prince, J.E., Cho, J.H., Dumontier, E., Andrews, W., Cutforth, T., Tessier-Lavigne, M.,
997 Parnavelas, J., and Cloutier, J.F. (2009). Robo-2 controls the segregation of a portion of
998 basal vomeronasal sensory neuron axons to the posterior region of the accessory
999 olfactory bulb. The Journal of neuroscience : the official journal of the Society for
1000 Neuroscience *29*, 14211-14222.
1001 Rahe, D.P., and Hobert, O. (2019). Restriction of Cellular Plasticity of Differentiated Cells
1002 Mediated by Chromatin Modifiers, Transcription Factors and Protein Kinases. G3
1003 (Bethesda) *9*, 2287-2302.
1004 Rothstein, M., and Simoes-Costa, M. (2020). Heterodimerization of TFAP2 pioneer
1005 factors drives epigenomic remodeling during neural crest specification. Genome Res *30*,
1006 35-48.
1007 Ryba, N.J., and Tirindelli, R. (1997). A new multigene family of putative pheromone
1008 receptors. Neuron *19*, 371-379.
1009 Seberg, H.E., Van Otterloo, E., Loftus, S.K., Liu, H., Bonde, G., Sompallae, R., Gildea,
1010 D.E., Santana, J.F., Manak, J.R., Pavan, W.J.*, et al.* (2017). TFAP2 paralogs regulate
1011 melanocyte differentiation in parallel with MITF. PLoS Genet *13*, e1006636.
1012 Silva, L., and Antunes, A. (2017). Vomeronasal Receptors in Vertebrates and the
1013 Evolution of Pheromone Detection. Annu Rev Anim Biosci *5*, 353-370.
1014 Silvotti, L., Cavaliere, R.M., Belletti, S., and Tirindelli, R. (2018). In-vivo activation of
1015 vomeronasal neurons shows adaptive responses to pheromonal stimuli. Scientific reports
1016 *8*, 8490.
1017 Skene, P.J., Henikoff, J.G., and Henikoff, S. (2018). Targeted in situ genome-wide
1018 profiling with high efficiency for low cell numbers. Nature protocols *13*, 1006-1019.
1019 Skene, P.J., and Henikoff, S. (2017). An efficient targeted nuclease strategy for high-
1020 resolution mapping of DNA binding sites. eLife *6*.
1021 Stefanakis, N., Carrera, I., and Hobert, O. (2015). Regulatory Logic of Pan-Neuronal
1022 Gene Expression in C. elegans. Neuron *87*, 733-750.

Stowers, L., Holy, T.E., Meister, M., Dulac, C., and Koentges, G. (2002). Loss of sex discrimination and male-male aggression in mice deficient for TRP2. Science *295*, 1493-1500.

Taroc, E.Z.M., Naik, A.S., Lin, J.M., Peterson, N.B., Keefe, D.L., Jr., Genis, E., Fuchs, G., Balasubramanian, R., and Forni, P.E. (2020). Gli3 Regulates Vomeronasal Neurogenesis, Olfactory Ensheathing Cell Formation, and GnRH-1 Neuronal Migration. The Journal of neuroscience : the official journal of the Society for Neuroscience *40*, 311-326.

Trouillet, A.C., Keller, M., Weiss, J., Leinders-Zufall, T., Birnbaumer, L., Zufall, F., and Chamero, P. (2019). Central role of G protein Galphai2 and Galphai2(+) vomeronasal neurons in balancing territorial and infant-directed aggression of male mice. Proc Natl Acad Sci U S A *116*, 5135-5143.

Trouillet, A.C., Moussu, C., Poissenot, K., Keller, M., Birnbaumer, L., Leinders-Zufall, T., Zufall, F., and Chamero, P. (2021). Sensory Detection by the Vomeronasal Organ Modulates Experience-Dependent Social Behaviors in Female Mice. Front Cell Neurosci *15*, 638800.

Vaddadi, N., Iversen, K., Raja, R., Phen, A., Brignall, A., Dumontier, E., and Cloutier, J.F. (2019). Kirrel2 is differentially required in populations of olfactory sensory neurons for the targeting of axons in the olfactory bulb. Development *146*.

Walz, A., Rodriguez, I., and Mombaerts, P. (2002). Aberrant sensory innervation of the olfactory bulb in neuropilin-2 mutant mice. The Journal of neuroscience : the official journal of the Society for Neuroscience *22*, 4025-4035.

Wankhade, S., Yu, Y., Weinberg, J., Tainsky, M.A., and Kannan, P. (2000). Characterization of the activation domains of AP-2 family transcription factors. The Journal of biological chemistry *275*, 29701-29708.

Weiler, E., McCulloch, M.A., and Farbman, A.I. (1999). Proliferation in the vomeronasal organ of the rat during postnatal development. The European journal of neuroscience *11*, 700-711.

Williams, C.M., Scibetta, A.G., Friedrich, J.K., Canosa, M., Berlato, C., Moss, C.H., and Hurst, H.C. (2009). AP-2gamma promotes proliferation in breast tumour cells by direct repression of the CDKN1A gene. EMBO J *28*, 3591-3601.

Wilson, K.C.P., and Raisman, G. (1980). Age-related changes in the neurosensory epithelium of the mouse vomeronasal organ: Extended period of post-natal growth in size and evidence for rapid cell turnover in the adult. Brain research *185*, 103-113.

Yu, G., Wang, L.G., Han, Y., and He, Q.Y. (2012). clusterProfiler: an R package for comparing biological themes among gene clusters. OMICS *16*, 284-287.

Yu, G., Wang, L.G., and He, Q.Y. (2015). ChIPseeker: an R/Bioconductor package for ChIP peak annotation, comparison and visualization. Bioinformatics *31*, 2382-2383.

Zhang, Y., Liu, T., Meyer, C.A., Eeckhoute, J., Johnson, D.S., Bernstein, B.E., Nusbaum, C., Myers, R.M., Brown, M., Li, W.*, et al.* (2008). Model-based analysis of ChIP-Seq (MACS). Genome biology *9*, R137.

Zuloaga, D.G., Morris, J.A., Monks, D.A., Breedlove, S.M., and Jordan, C.L. (2007). Androgen-sensitivity of somata and dendrites of spinal nucleus of the bulbocavernosus (SNB) motoneurons in male C57BL6J mice. Hormones and behavior *51*, 207-212.

FIGURE LEGENDS

Figure 1: Analysis of single cell sequencing data of the vomeronasal organ. P10 male controls shows the developing vomeronasal neurons as they progress through A-C) neurogenesis (Ascl1, Neurog1, Neurod1), D-E) maturation (Gap43, OMP), and F-I) apical and basal differentiation (Bcl11b, Tfap2e, Meis2). A) Ascl1 is expressed by transiently amplifying progenitor cells (cyan arrow), which transition into the immediate neuronal precursors that turn on pro-neural genes (cyan arrow) Neurog1 (B) and Neurod1 (C) and turn off as the precursors turn into immature neurons (black and magenta). D) Immature neurons express Gap43, which persists in both apical (black arrow) and basal (magenta arrow) branches, until it declines as neurons begin to reach maturity and express E) OMP in mature apical (black arrow) and mature basal (magenta arrow) VSNs. Gap43 and OMP expression briefly overlap, as the neurons transition to a fully differentiated mature stage. F) Bcl11b mRNA expression is found in both apical and basal VSNs but at different developmental timepoints. Bcl11b is found in committed basal precursors near the establishment of the apical/basal dichotomy (magenta arrow) but is not found until later in apical VSN development (black arrow) G) AP-2ε is expressed by the basal branch (magenta arrows) and H) Meis2 mRNA expression is found in the apical branch (black arrows) and even in early neurogenesis stages (cyan arrow), and their expression does not overlap. J) Enhanced volcano plot. Differential gene expression between apical and basal branches of VSNs. Apical specific genes (55 genes) trend left and basal specific genes (187 genes) trend right. Significance defined as Log_2-Fold Change > 0.3 and Adjusted p-value ≤ 0.05.

Figure 2: KO mouse generation and characterization of rescued AP2e expression. A) Knock-in strategy through homologous recombination to generate the R26AP2ε mouse line. The CAG-loxP-stop-loxP-mouse-Tfap2e cassette as integrated into the first intron of Rosa26 B-C) Immunohistochemistry on P21 wild-type (B, E, H), AP-2εNull (C, F, I), and AP-$2\varepsilon^{Rescue}$ (D, G, J) mice against AP-2ε and Cre recombinase. B-B') In WT mice AP-2ε expression is in the marginal zones (MZ) and in the basal regions of the VSNs. C) In AP-$2\varepsilon^{Null}$ mice, no AP-2ε immunoreactivity is observed but lost in the central regions where more mature neurons reside. D) In the AP-$2\varepsilon^{Rescue}$, AP-2ε expression in the basal region, but with less intensity and density at the tips compared to WT controls. E-G) Immunostainings against V2R2 (magenta) and Meis2 (green) counterstained with DAPI (white). H-J) Immunostainings against Gαo (magenta) and Gαi2 (green) counterstained with DAPI). K) AP-2εNull mice show a dramatic reduction in basal VSNs and apical VSNs occupy most of the epithelium (E, F, H, I, K). D, G, J, K) The AP-$2\varepsilon^{Rescue}$ has an intermediate phenotype between WT and AP-$2\varepsilon^{Null}$ mice, where the VNE contains more basal VSNs than in the AP-$2\varepsilon^{Null}$ mice but does not reach the equivalency of the WT (K).

Figure 3: Territorial aggression and sex preference depends on AP-2ε expression in mice. A) The odorant preference paradigm where cotton swabs with either male or female whole urine are placed on opposite ends of a test cage and the amount of time spent smelling each odorant is measured. B) Male wild-type mice spent significantly more

time investigating female odorants than male odorants. Preference for female odorants is lost in AP-2ε KO male mice but restored in AP-2ε rescue mice. C) Male-male aggression was evaluated using the Resident intruder paradigm B) Wild-type mice display aggressive behaviors toward male intruders and number of attacks were quantified. C) AP-2ε Null mice attacked intruders significantly less than WT mice. However, AP-2ε Rescue mice showed significantly more aggressive behaviors that is not significantly different than the WT male mice. G) Seminal vesicle weight was not significantly different across all genotypes when normalized to bodyweight.

Figure 4: Ectopic expression of AP-2ε in the MOE and the VNE promotes expression of basal markers. Immunostainings at P10 on OMPCre$^{+/-}$ controls (A-D) and OMPCre$^{+/-}$/R26AP2ε$^{+/-}$ mutants (E-H). A) IHC against AP-2ε in the VNOs of shows that AP-2ε is expressed in only the basal VSNs (arrow) in Controls but have extended AP-2ε immunoreactivity into apical (magenta arrowheads) and sustentacular regions (white arrowheads) in the Ectopic mutant. B,F) ISH against Gαo show that in controls (B) Gαo mRNA expression is restricted to the basal regions of the VNE. F) Ectopic AP-2ε mutants show Gαo mRNA reactivity in the apical regions of the VNE (magenta arrowheads). C,G) Immunohistochemistry against V2R2 in the VNO of controls (C) shows no immunoreactivity in the apical regions of the VNE in controls (notched arrows) and is limited to the basal VSNs (black arrow). G) In mutants, more of the vomeronasal epithelium was positive for V2R2 in mutants, as expression expands into the apical regions of the epithelium (magenta arrowheads). D-H') P10 VNOs immunostained against Gαo (green) and V2R2 (magenta) show that Gαo and V2R2 colocalize almost completely in the basal regions of the VNE. OMPCre$^{+/-}$/R26AP2ε$^{+/-}$ mutants have Gαo/V2R2 positive VSNs localized in apical regions of the VNE. I-J) Violin plot of Gαo (I), and Vmn2r7 (J) mRNA expression between apical and basal VSNs in OMPCre$^{+/-}$ controls and apical VSNs of OMPCre$^{+/-}$/R26AP2ε$^{+/-}$ mutant mice show significant upregulation of basal markers based on p.value ($p<0.05$ = *, $p<0.0004$ = ****). K,L) Quantifications at P10 show a significant increase in the amount of the neuroepithelium positive for V2R2 (I) and Gαo (J). Quantifications at P21 show significantly more of the epithelium is V2R2+. (K) The amount of the epithelium positive for Gαo is not significantly different between genotypes (L). M, O) Immunofluorescence against V2R2 (magenta) and Meis2 (green) in controls (M) and OMPCre$^{+/-}$/R26AP2ε$^{+/-}$ mutants (O). N, P) Immunofluorescence against Gαo (magenta) in control (N) and OMPCre$^{+/-}$/R26AP2ε$^{+/-}$ mutant (P). Q) Our quantifications show that ectopic mutants have significantly more cells positive for basal markers in the apical regions than controls.

Figure 5: Progressive changes in VNE lamination may reflect the changing expression profiles of cell adhesion molecules in apical VSNs. Immunofluorescence against Sox2 (cyan), AP-2ε (magenta), and Meis2 (green) with DAPI (blue) counterstain. Neuroepithelium traced in yellow dotted line. A) P21 WT Controls show highly organized stratified neuroepithelium with contiguous layers of AP-2ε+/basal (magenta), Meis2+/apical (green), and Sox2+/sustentacular cell (cyan) layers. B-C) OMPCre$^{+/-}$ /R26AP2ε$^{+/-}$ VNO at B) P21 show that Sox2+/sustentacular cells have intraepithelial cysts

with internalized subsidiary lumens (red arrows) C) In adults (3mo) OMPCre$^{+/-}$/R26AP2ε$^{+/-}$ mutants show an increase in the severity of intraepithelial cysts (red arrows) and breaks in the sustentacular layer and expansion of neurons to the luminal surface (red notched arrows). Unidentified matter (*) reactive to anti-mouse Abs was detected within the cysts. D) Quantifications of the zonal distribution through Zone 1 (dorsal) -> Zone 7 (ventral) of these cytoarchitecture abnormalities (which include both cell body abnormalities and dendritic disorganization, each point = 1 animal) show that these disruptions occur in the intermediate and central regions of the VNO, but not in the marginal zones (MZ, Zone1,7). The highest rate of occurrence are in zone 3 and 6, which are intermediate regions in the VNO. E) Dot plot showing that composition and intensity of differentially expressed genes involved in cellular adhesion in the VSNs of controls and ectopic AP-2ε mutants.

Figure 6: Single-cell sequencing of P10 OMPCre$^{+/-}$ control and OMPCre$^{+/-}$R26AP2ε$^{+/-}$ mutant VSNs indicate a shift in apical cells towards basal cells in the mutant. A-A’’’) UMAP clustering of VSNs from progenitor cells to differentiated mature apical and basal cells of Control B-B’’’) Mutant mice split by genotype. A’-A’’’, B’-B’’’) Blended feature plots of AP-2ε expression (red) and Meis2 (blue). Red arrowheads indicate onset of AP-2ε expression. Black arrow indicates mature apical VSNs. OMPCre$^{+/-}$ Controls (A’-A’’’) show a divergent pattern of expression where the onset of AP-2ε (red, red arrowhead) is only on the basal branch. Meis2 expression (blue) occurs only on the apical branch where the cells lack AP-2ε expression. OMPCre$^{+/-}$R26AP2e$^{+/-}$ mutants (B’-B’’’) start to express AP-2ε on the basal branch in immature basal VSNs, however, onset of AP-2ε mRNA expression also occurs on the apical branch where OMP expression begins (red arrowhead). AP-2ε mRNA is co-expressed with Meis2 mRNA in in apical VSNs from ectopic mutants (red arrowhead arrow). We found that these cells clustered separately from mature apical cells from the control and mature basal cells from the mutant but are a unique population that bridge the gap between normal apical and basal cells (arrows). D) Violin plot shows Calreticulin (Calr) mRNA expression levels in apical VSNs from the OMPCre$^{+/-}$R26AP2ε$^{+/-}$ mutants are reduced to levels similar to basal VSNs from OMPCre$^{+/-}$ controls. E) Violin plot shows Calreticulin-4 (Calr4) mRNA expression levels. E) In control cells, AP-2ε mRNA expression (red arrowheads) and Meis2 mRNA expression (blue) are not co-expressed in the same cells. AP-2ε expression is upregulated in immature basal VSNs and not apical VSNs. F-G) ISH against Calr4 against P11 OMPCre$^{+/-}$ controls(G) and OMPCre$^{+/-}$R26AP2ε$^{+/-}$ mutants (G) show that while Calr4 mRNA is normally enriched in basal VSNs (arrowheads), ectopic AP-2ε mutants show expansion of Calr4 positivity in the apical regions when compared to controls (arrows). H-K) Analysis of CUT&RUN against Tfap2e/AP-2ε. H) Tornado plot of AP-2ε occupancy in the dissociated tissue of the VNO. The genomic regions are defined as the summit +/- 1kb. I) Pie chart depicting the genomic distribution of putative AP-2ε binding sites show that most of AP-2ε peaks are found in promoter regions of putative target genes and to a lesser extent in intergenic and intronic regions of the genome. J) Venn diagram of the determined AP-2ε targets and the genes enriched in the basal and apical VSNs. K) Venn diagram of the determined AP-2ε targets and all the upregulated and downregulated genes in the ectopic AP-2ε mutant mouse. Significance defined by Adjusted p-value ≤ 0.05.

Figure 7: Ectopic AP-2ε expression alters the detection of sex-specific odorants. A-D) Immunofluorescence against pS6 (magenta, arrows) and Meis2 (green) with DAPI counterstain (blue) in the VNE of Controls (A,C) and OMPCreR26AP-2ε mutants (B,D). A-B) VNE of adult male wildtype and ectopic mutants when exposed to male soiled bedding show similar activation or pS6 immunoreactivity (arrows) in Meis2+/apical and Meis2-/basal VSNs. C,D) VNE of adult female wildtype and ectopic mutants when exposed to female soiled bedding show the while WT females displayed a higher proportion of pS6+ apical VSNs OMPCre$^{+/-}$/R26AP-2ε$^{+/-}$ mutants showed a decreased number of activated Meis2+/apical VSNs. In both exposure conditions ectopic activation of sustentacular cells (notched arrows) and VSNs near the lumen (arrowheads). E) Quantifications of activated VSNs in male mice after exposure to male-soiled bedding show similar activation between mutants and controls. Small but non-significant increase in the total number of activated basal VSNs. F) Quantifications of activated VSNs after exposure to sex-specific odorants in female mice show a significant decrease in the number of activated apical VSNs with no change in the number of activated VSNs between female OMPCre$^{+/-}$/R26AP-2ε$^{+/-}$ mutants and controls. G) Quantifications of the number of attacks for all WT and OMPCre$^{+/-}$/R26AP-2ε$^{+/-}$ mutants in a resident intruder test show male ectopic AP-2ε mice display higher levels of intermale aggression, but are not significantly different than controls. H) Quantifications of odorant preference tests in male and female mice show that male and female OMPCre$^{+/-}$/R26AP-2ε$^{+/-}$ mutants retain the preference for opposite sex odorants. Significance defined as p-value ≤ 0.05.

SUPPLEMENTARY FIGURE LEGENDS

Supplementary Figure S1: Expression of potential AP-2 co-factors in both apical and basal VSNs. Featureplots of known AP-2 family cofactors p300/CBP, Cited2, Cited4, Kctd1, Sp1, Sp8, Yy1 in P10 VSNs.

Supplementary Figure S2: **AP-2ε and V2R2 immunoreactivity in the MOE.** P10 OMPCre$^{+/-}$ controls(A,C) and OMPCre$^{+/-}$/R26AP-2ε$^{+/-}$ ectopic mutants (B,D). A-B) Immunohistochemistry against AP-2ε in the main olfactory epithelium (OE) shows no immunoreactivity in controls (black notched arrows) and ectopic AP-2ε expression in the mutants (magenta arrowheads). C-D) Immunohistochemistry against V2R2 in the main olfactory epithelium (OE) shows no expression in either control (C) nor ectopic AP-2ε mutant (D).

Supplementary Figure S3: Analysis of Sustentacular Cells. A-F) Immunofluorescence on Wildtype (A-C) and OMPCre$^{+/-}$/R26AP2ε$^{+/-}$ mutants (D-F) against AP-2ε (magenta) and Sox2 (green) counterstained with DAPI (blue). A-C) A-C) WT controls and ectopic AP-2ε mutants (D-F) show sustentacular (sus) cells with high immunoreactivity for Sox2 and no AP-2ε expression. Apical (a) VSNs closest to the sustentacular cell layer show low immunoreactivity for Sox2 (brackets, arrowheads) with apical VSNs closer to basal (b) VSNs with no immunodetectable Sox2 (notched arrows). no colocalization between AP-2ε and Sox2+ sustentacular cells (sus). D-F) OMPCre$^{+/-}$ /R26AP2ε$^{+/-}$ mice have some Sox2+ sustentacular cells that have ectopic AP-2ε expression (arrows). G) UMAPs of sustentacular cells from OMPCre$^{+/-}$/R26AP2ε$^{+/-}$ adults showed that AP2ε positive and negative clusters segregated from each other with accompanying feature plots showing the expression of sustentacular cell markers Hes1, Krt8, and Cyp2a5 along with ectopic Tfap2e/AP-2ε mRNA expression. H) Gene ontology analysis of Tfap2e+ sustentacular cells showed an enrichment of dysregulated genes related to cytoskeleton organization, cell-cell junction organization, cytoskeletal organization, and cytoplasmic ribosomal proteins. I) Heatmap of up- and down-regulated genes found related to cytoskeleton organization, cell-cell junction organization, and cytoskeleton organization in Tfap2e positive and negative sustentacular cells.

Supplementary Figure S4: Analysis of the AOBs from adult WT and OMPCre$^{+/-}$ /R26AP2ε$^{+/-}$ mice. A-B) Immunofluorescence against Nrp2 (green) and Robo2 (red) and counterstained with DAPI (blue) showed that the expression of guidance cue molecules in WT (A) and OMPCre$^{+/-}$/R26AP2ε$^{+/-}$ (B) mice was comparable and showed distinct anterior and posterior AOB regions (arrows). C,D) Immunofluorescence against Kirrel2 (green) and Kirrel3 (red) and DAPI (blue) counterstain on WT (C) and OMPCre$^{+/-}$ /R26AP2ε$^{+/-}$ (D) AOBs showed the glomerular organization and morphology was comparable between genotypes (arrows). Similar E) Quantifications of the average area of the AOB was not significantly different across genotypes. Analysis of the glomeruli size (F) and number (G) using IF against Kirrel2 and Kirrel3 showed no significant changes across genotypes.

Supplementary Figure S5: A) AP-2ε binding in WT and OMPCreR26AP2ε mutants at TSS of apical and basal enriched genes and the significantly up- and down-regulated genes in the OMPCreR26AP2ε mutants. B) AP-2ε enrichment at putative activated and repressed target genes in the OMPCreR26AP2ε ectopic mutant shows greater enrichment at up-regulated targets. C) Dot plot of enriched GO terms show many putative AP-2ε target genes being chromatin or histone modifiers. D) Motif enrichment analysis validated our analysis as Tfap2 was the top motif found at putative binding sites. It also yielded TF family motifs of potential cofactors including SP, KLF, EBF, RFX, ELK, NRF, DLX, and LHX transcription factor families. E) Tracks from CUT&RUN sequencing where AP-2ε peaks are found in the promoter regions of activated (purple) and repressed (yellow) genes.

Supplementary Figure S6: Differential gene expression analysis from scSeq in adult animals of apical and basal populations scSeq in Adults WT Controls and OMPCre$^{+/-}$/R26AP2ε$^{+/-}$ VNOs. A) Volcano Plot of significantly up- and down-regulated genes in apical VSNs in adult WT and OMPCre$^{+/-}$/R26AP2ε$^{+/-}$ mice show dysregulation of many key basal genes and down-regulation of apical-enriched genes. B) Volcano Plot of significantly up and downregulated genes in basal VSNs in adult WT and OMPCre$^{+/-}$ /R26AP2ε$^{+/-}$ mice show that some genes may respond to AP-2ε regulation in a dose-dependent manner. C) Dot plot of canonical genes expressed by apical and basal VSNs and key genes identified in scSeq analysis for P10 and Adult Control and Mutant mice.

SUPPLEMENTARY TABLES

Supplementary Table S1:
Genes enriched in apical and basal populations of VSNs
Significance defined as Adjusted p-value ≤ 0.05

Supplementary Table S2:
Significantly dysregulated genes in apical VSNs from OMPCreR26AP2ε mice
Significance defined as Adjusted p-value ≤ 0.05

GRAPHICAL ABSTRACT

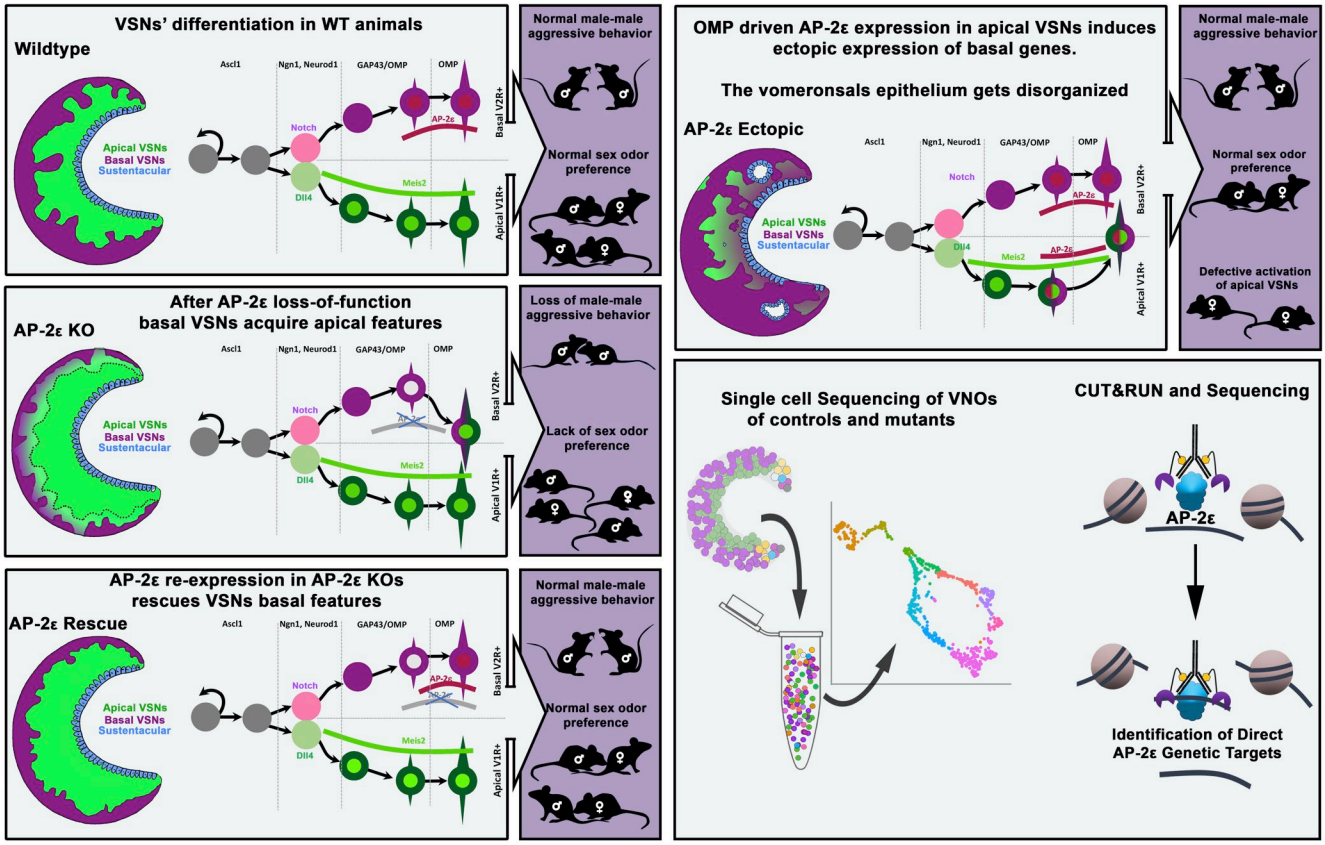

FIGURE 1

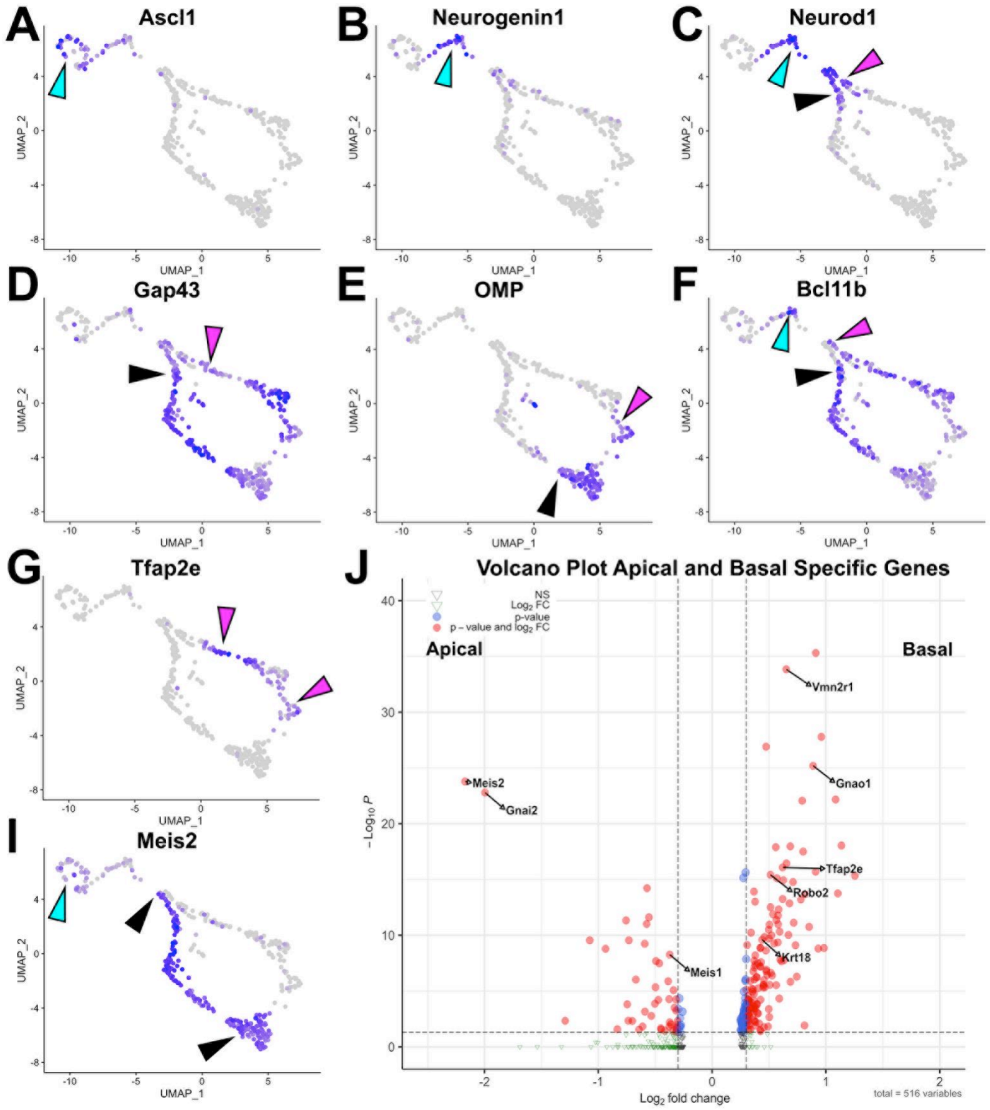

1331 **FIGURE 2**

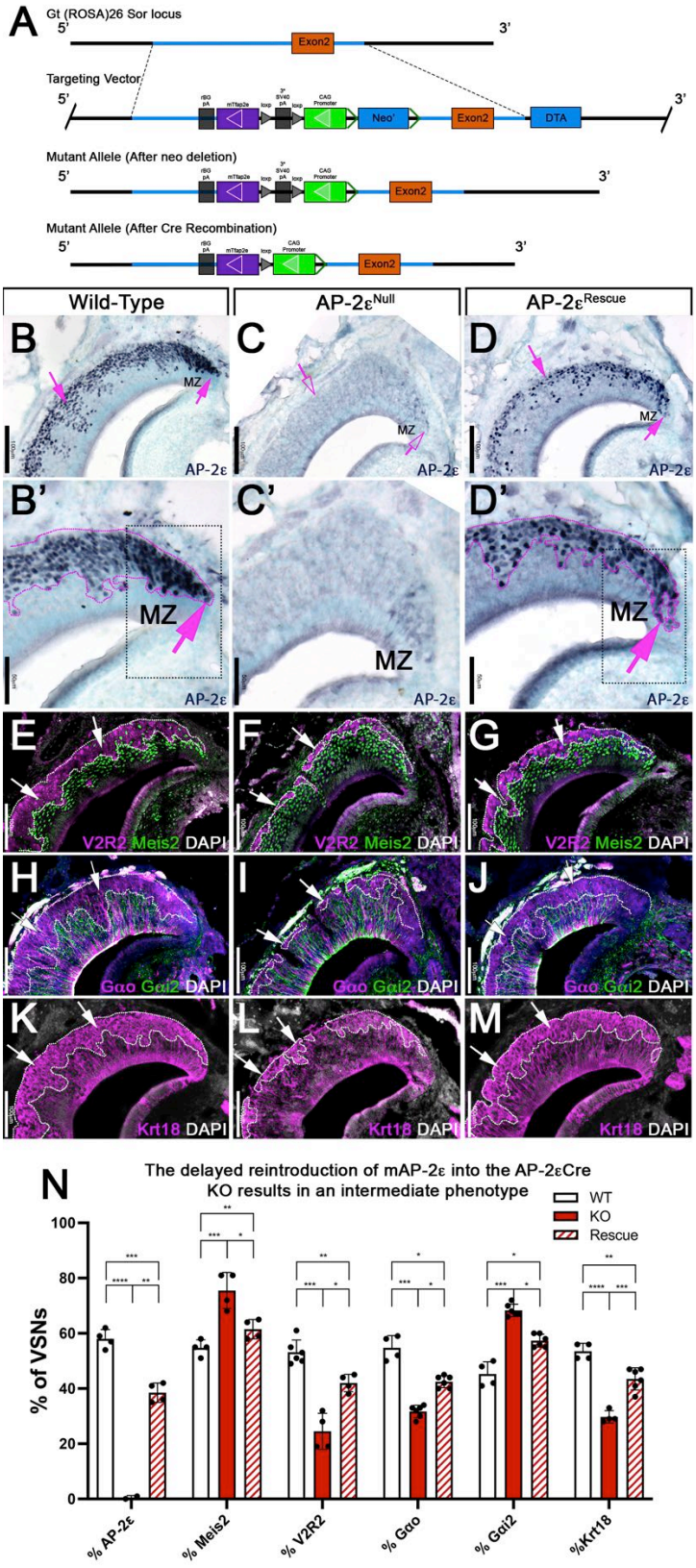

1332
1333

1334 **FIGURE 3**

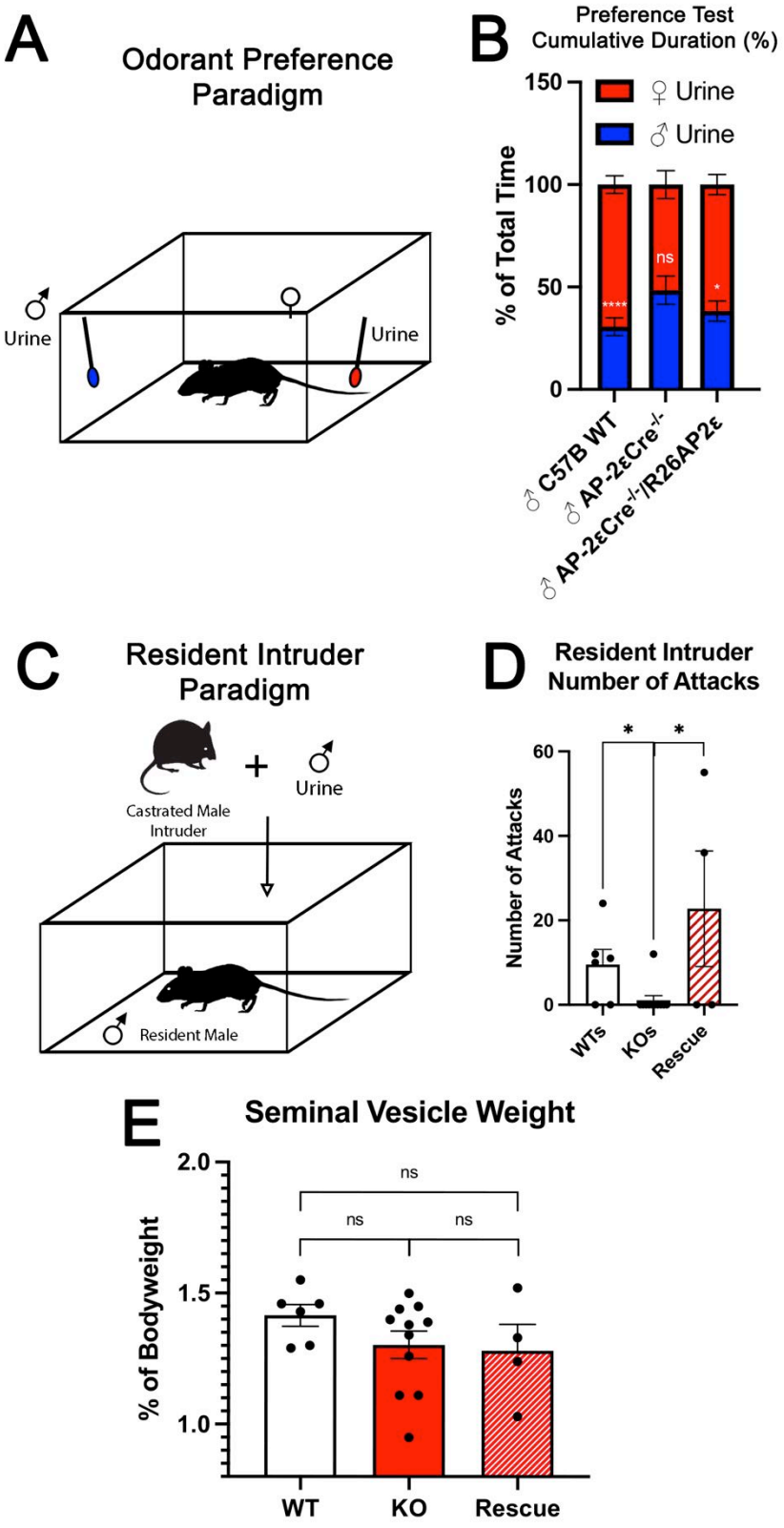

1335

FIGURE 4

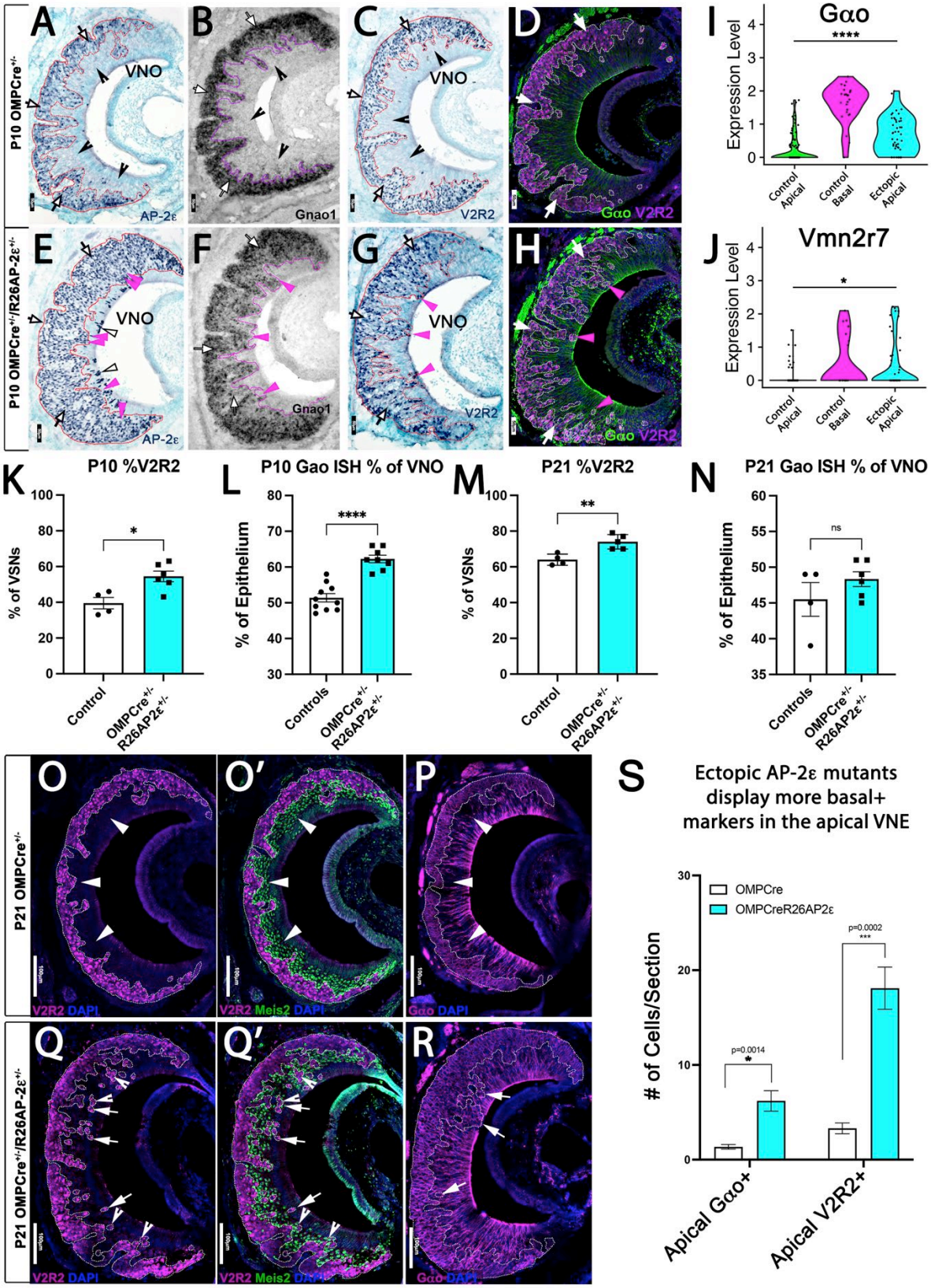

FIGURE 5

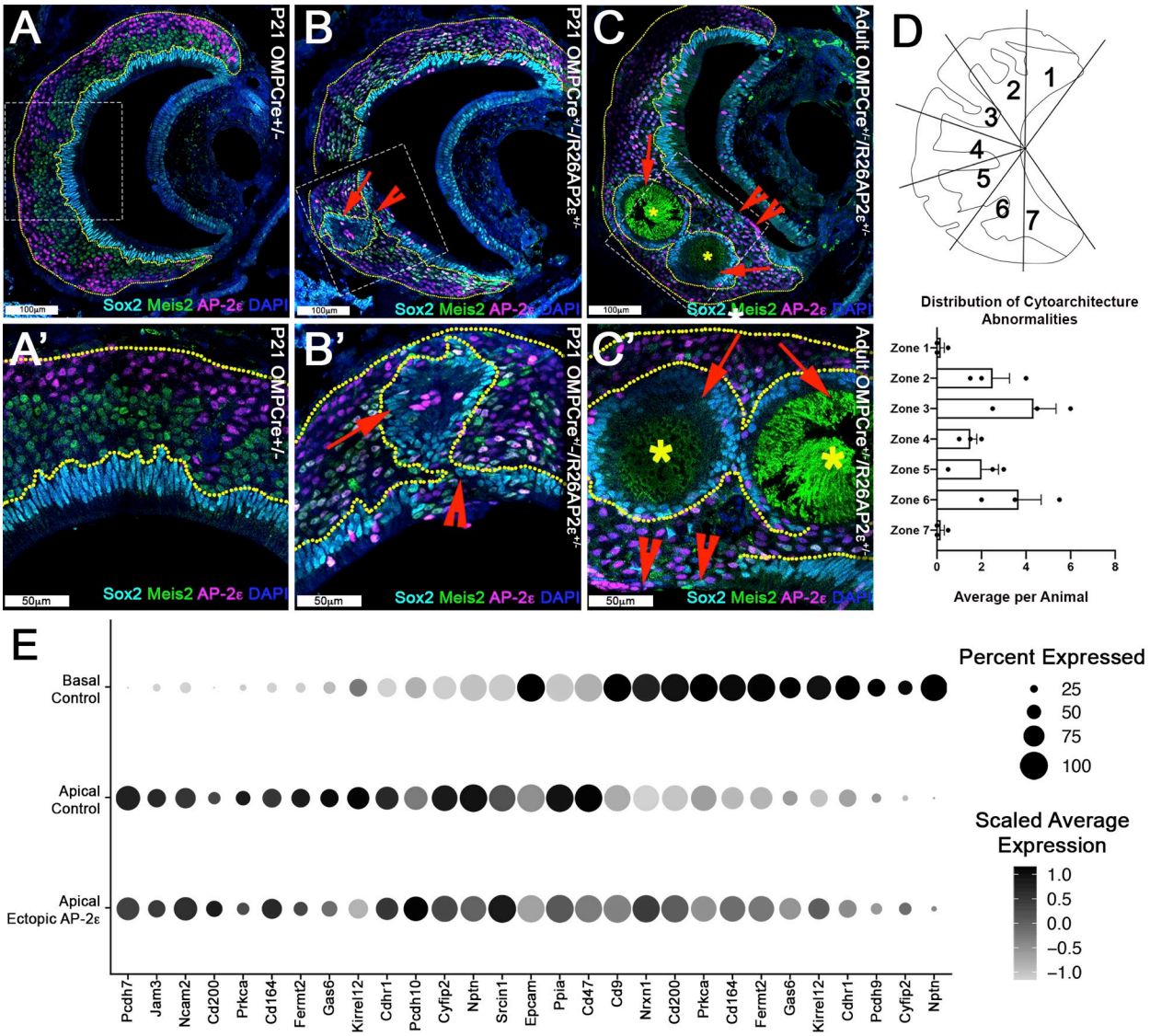

FIGURE 6

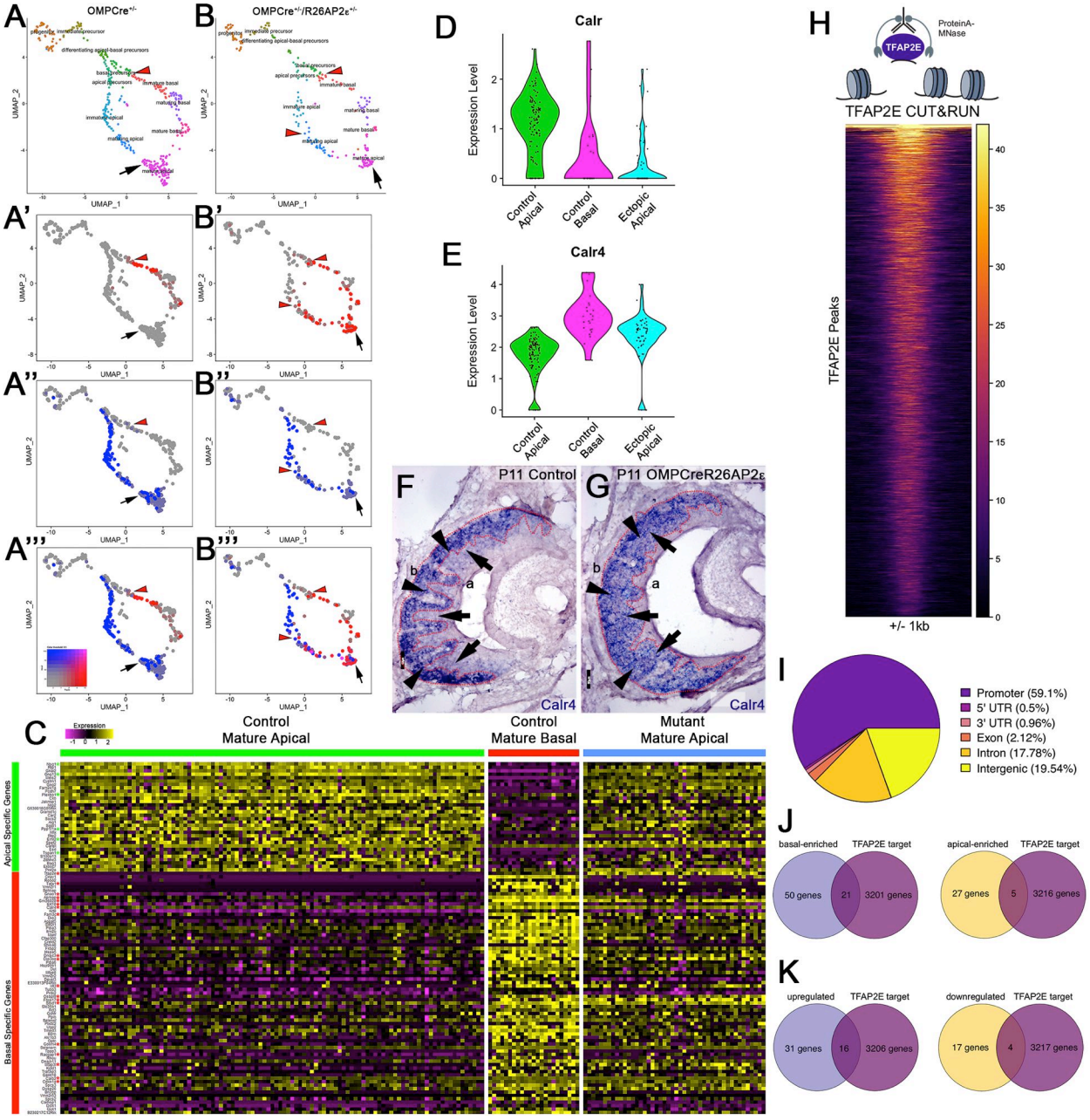

1356 **FIGURE 7**

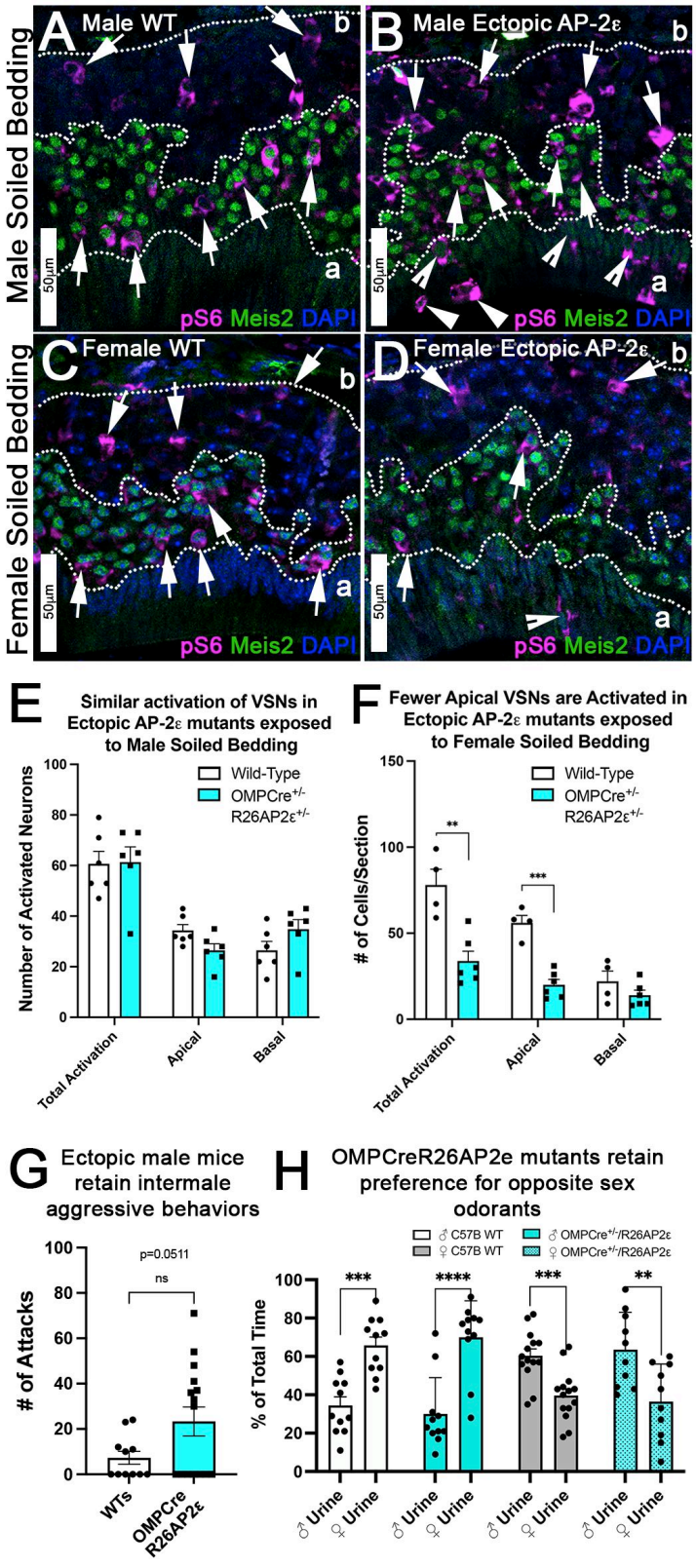

1357
1358

SUPPLEMENTARY FIGURES

FIGURE S1

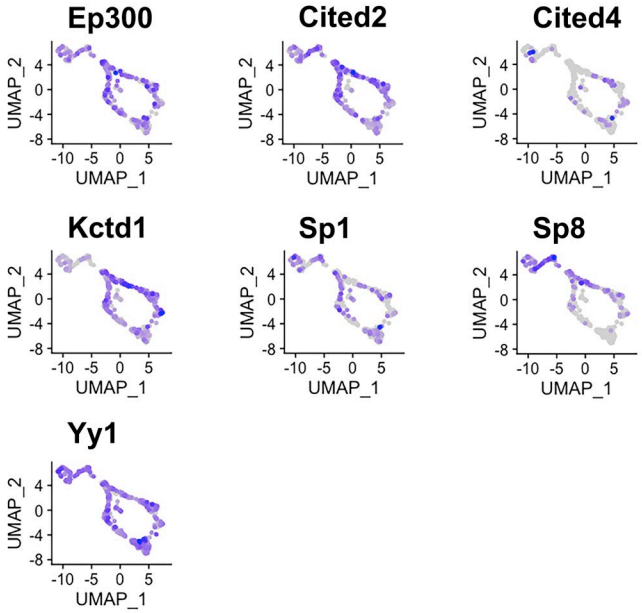

FIGURE S2

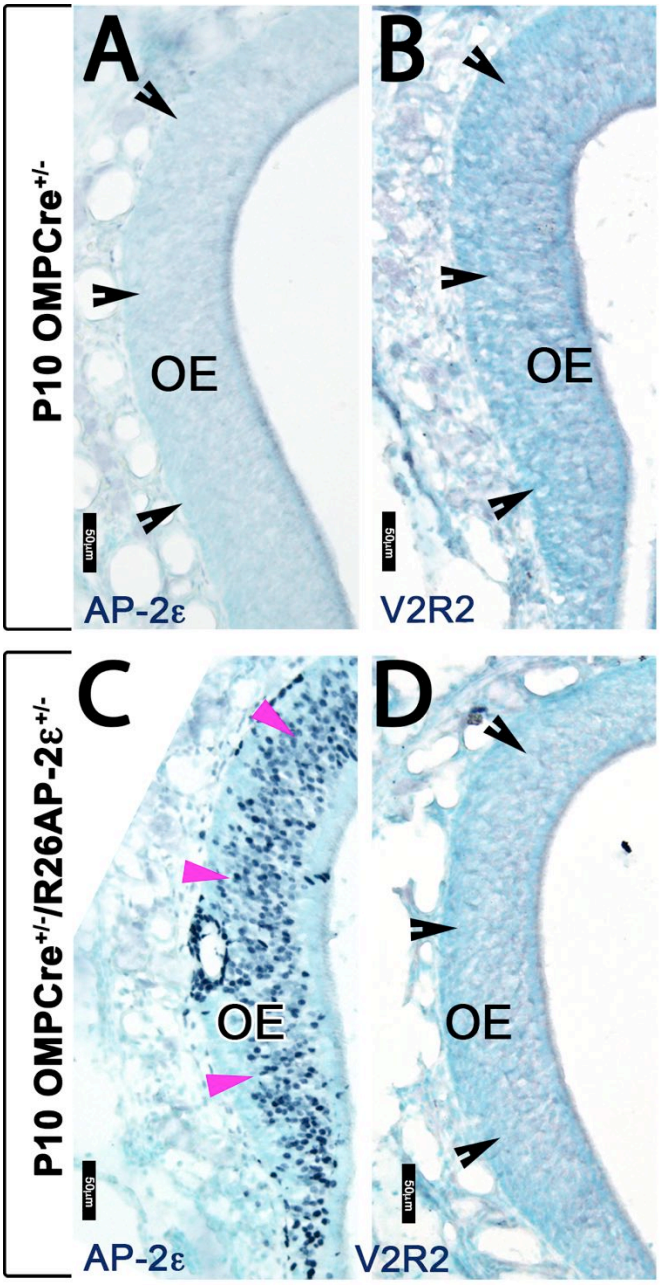

FIGURE S3

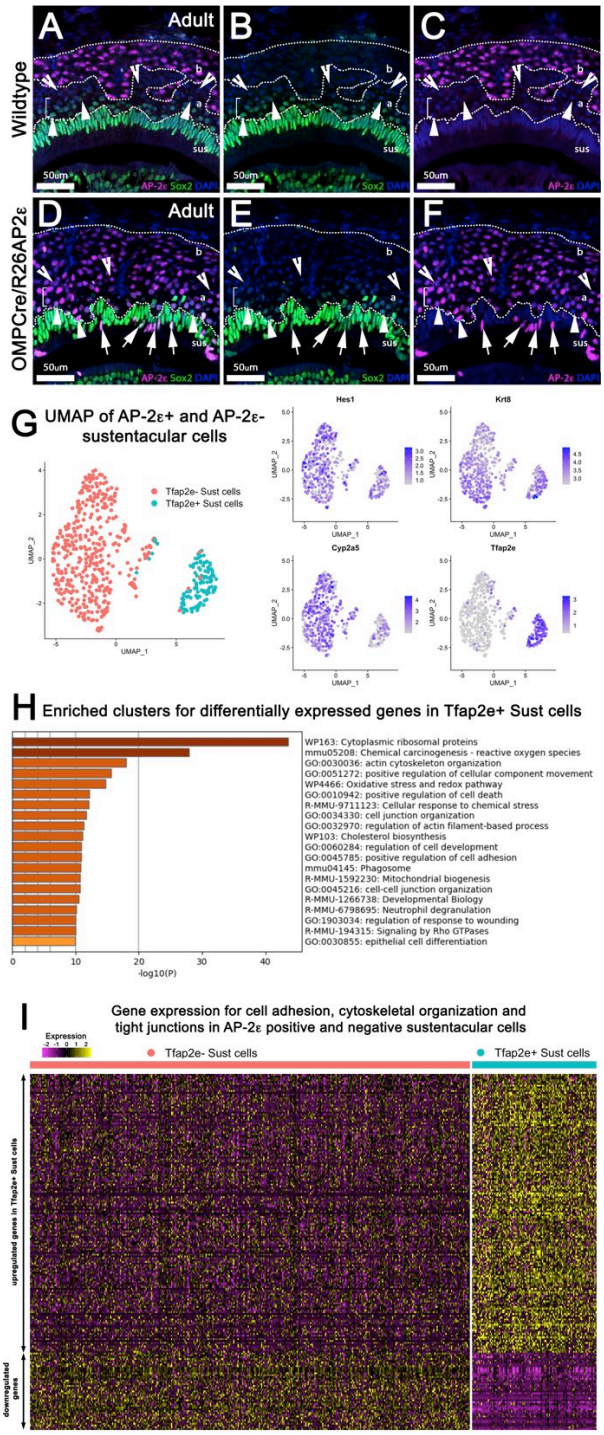

FIGURE S4

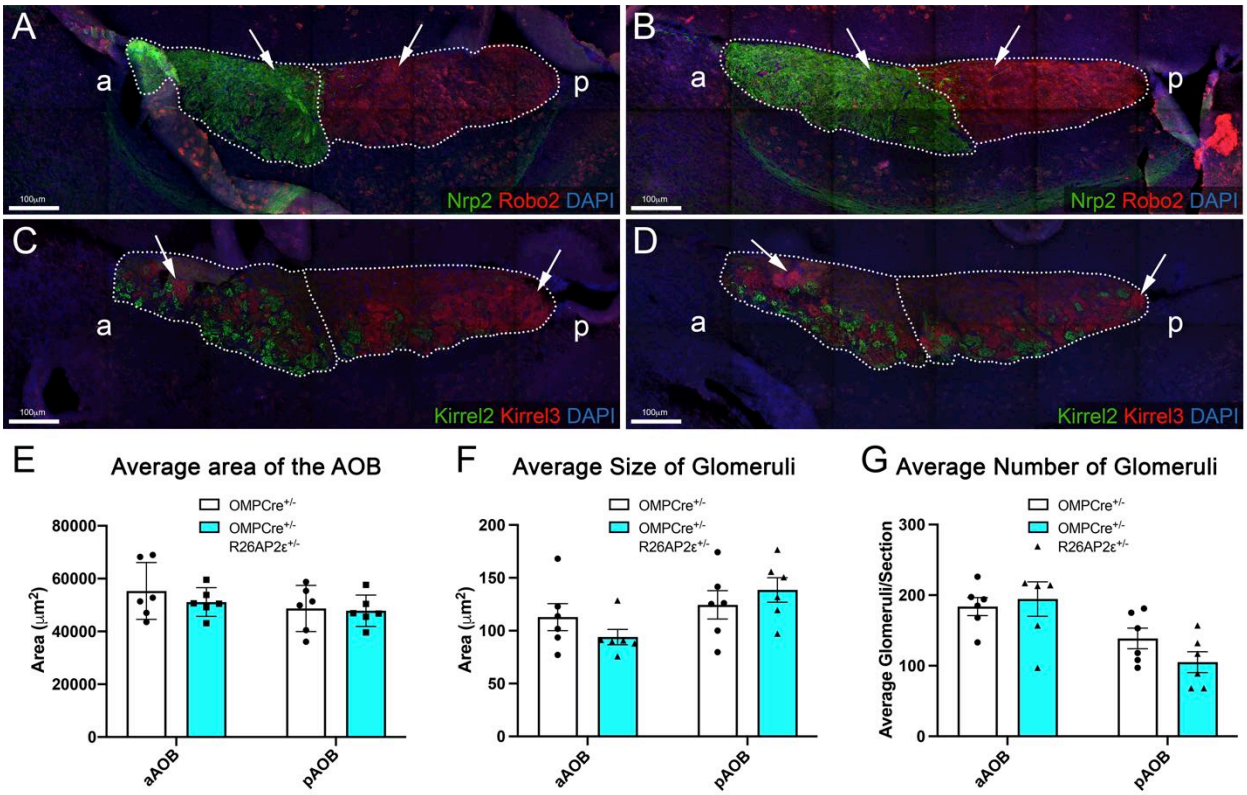

FIGURE S5

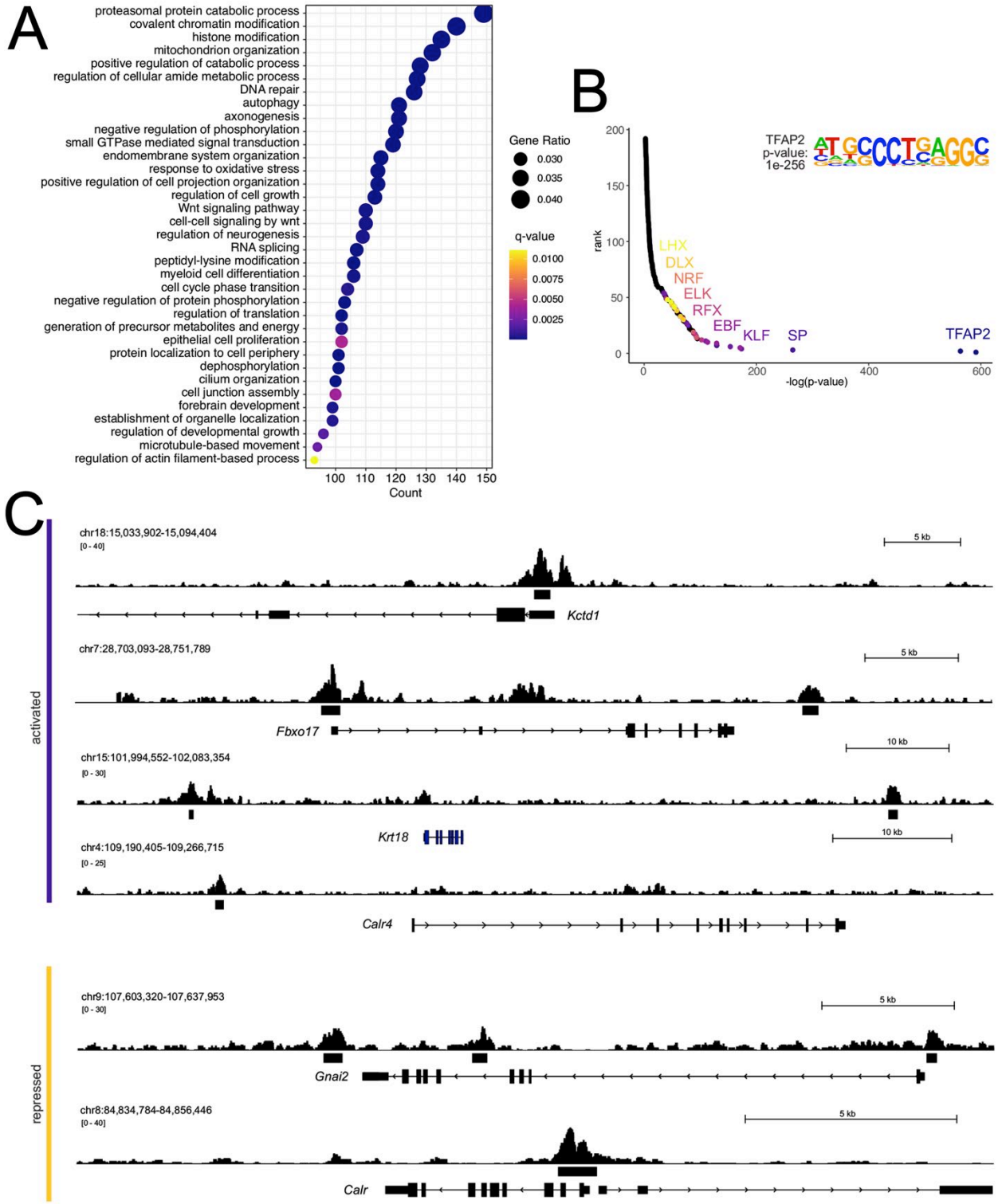

FIGURE S6

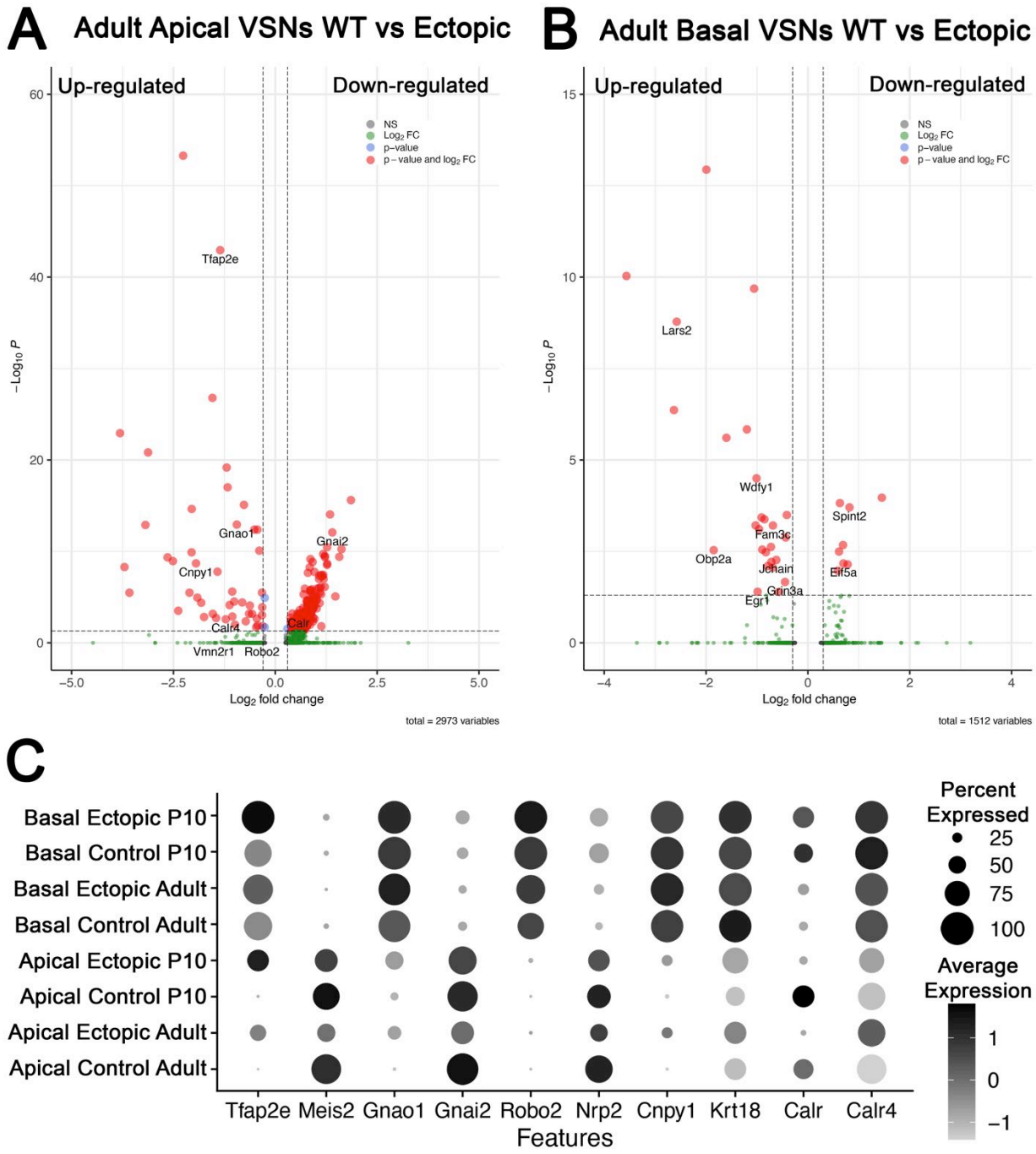

Supplementary Table S1

Differentially expressed genes in mature apical and basal VSNs

Apically Enriched Genes					
Gene Name	P. Value	Average Log Fold Change	Mature Basal %	Mature Apical %	Adjusted P.Value
Nsg1	2.19E-13	-1.9461937	0.87	0.991	4.77E-09
Rtp1	3.99E-13	-1.7210806	0.13	0.972	8.69E-09
Gnai2	1.21E-12	-3.2758293	0.261	0.963	2.63E-08
Gng13	1.44E-12	-2.4998775	0.565	0.981	3.14E-08
Meis2	1.46E-12	-2.3994924	0.087	0.944	3.18E-08
Cystm1	2.60E-12	-1.1223905	0.913	1	5.66E-08
Gng2	4.70E-12	-1.8780287	0.696	0.963	1.02E-07
Fam241a	2.15E-11	-1.3441602	0.304	0.925	4.68E-07
Pcdh7	5.79E-11	-1.1606574	0.043	0.869	1.26E-06
Plekhb1	3.29E-10	-0.8073116	0.739	0.991	7.16E-06
Ckb	5.70E-10	-0.942904	0.957	1	1.24E-05
Jakmip1	2.13E-09	-0.7864416	0.13	0.841	4.65E-05
Nrp2	2.48E-09	-0.9997662	0.565	0.925	5.41E-05
G630016G05Rik	3.62E-09	-0.8518453	0	0.766	7.89E-05
Gramd1c	6.12E-09	-0.8132581	0.304	0.869	1.33E-04
Car2	1.29E-08	-0.871219	0.783	0.963	2.82E-04
Socs2	1.40E-08	-0.8762327	0.913	0.981	3.04E-04
Aig1	1.33E-07	-0.6442775	0.478	0.869	2.91E-03
Sgpl1	1.38E-07	-0.750675	0.652	0.953	3.01E-03
Ppp1r1a	1.62E-07	-0.6387545	0.87	0.953	3.53E-03
Nfix	1.63E-07	-0.6919687	0.087	0.71	3.55E-03
Rtp2	2.67E-07	-0.6124008	0.783	0.925	5.81E-03
Eml2	3.24E-07	-0.4522206	0	0.645	7.05E-03
Spef2	3.76E-07	-0.6257323	0.522	0.907	8.19E-03
Cartpt	6.02E-07	-0.504793	0.957	0.963	1.31E-02
Esd	6.05E-07	-0.5783619	0.174	0.748	1.32E-02
Tspan1	7.99E-07	-0.6642304	0.304	0.785	1.74E-02
S100a13	1.18E-06	-0.6578302	0.217	0.72	2.58E-02
Zdhhc3	1.22E-06	-0.6494611	0.609	0.879	2.65E-02
Bag1	1.60E-06	-0.4936463	0.87	0.972	3.48E-02
Exosc7	1.70E-06	-0.4935659	0.522	0.841	3.71E-02
Prxl2a	1.95E-06	-0.6048927	0.957	1	4.24E-02

Basally Enriched Genes					
Gene Name	P. Value	Average Log Fold Change	Mature Basal %	Mature Apical %	Adjusted P.Value
Tfap2e	2.71E-23	1.01282475	0.87	0.019	5.90E-19
Cnpy1	1.23E-22	2.05509001	1	0.093	2.69E-18
Robo2	3.77E-22	0.90330448	0.957	0.056	8.20E-18
Tafa1	4.72E-21	0.96728089	0.826	0.028	1.03E-16
Vmn2r1	2.11E-19	1.2793116	0.783	0.028	4.59E-15
Sphkap	6.49E-15	0.28031925	0.522	0	1.41E-10
Gnao1	6.12E-14	1.42314493	0.957	0.327	1.33E-09
Apmap	1.17E-13	1.58179511	1	0.916	2.55E-09
Gm36028	1.19E-13	2.53665489	1	0.682	2.58E-09
Krt18	2.60E-13	1.6051759	1	0.673	5.67E-09
Calr4	6.57E-13	1.39565197	1	0.916	1.43E-08
Krt8	1.51E-12	1.68676872	0.957	0.551	3.28E-08
Fam3c	1.65E-12	1.07729387	1	0.664	3.60E-08
Dio3	1.68E-12	0.40528977	0.478	0.009	3.65E-08
Agpat5	1.79E-12	1.08439932	1	0.514	3.89E-08
Sdf2l1	5.07E-12	1.50705224	1	0.879	1.10E-07
Pdia3	6.16E-12	0.86129121	1	1	1.34E-07
Itm2b	7.96E-12	1.18425959	1	1	1.73E-07
Manf	1.07E-11	1.37611844	1	0.953	2.33E-07
Cfap300	2.16E-11	0.77700954	0.957	0.421	4.71E-07
Creld2	2.17E-11	1.00229149	0.957	0.523	4.73E-07
Shisa8	2.58E-11	0.36615576	0.391	0	5.63E-07
Fkbp2	2.90E-11	0.72341813	1	0.907	6.32E-07
Hspa5	5.22E-11	1.40010137	1	0.981	1.14E-06
Dnajc3	6.37E-11	1.1592286	0.957	0.729	1.39E-06
Dio3os	7.37E-11	0.49488572	0.565	0.047	1.60E-06
Pdia6	1.07E-10	1.14235131	1	0.888	2.32E-06
Hsp90b1	2.05E-10	0.85553036	1	0.991	4.47E-06
Dut	2.84E-10	0.76430257	1	0.86	6.19E-06
Mfge8	3.07E-10	1.07748862	0.957	0.794	6.68E-06
Vmn2r2	4.22E-10	1.35916407	0.391	0.009	9.19E-06
Dpysl3	1.30E-09	1.17193306	0.957	0.757	2.84E-05
E330013P04Rik	1.41E-09	0.35778211	0.609	0.084	3.08E-05
Mt3	1.88E-09	0.57279227	0.739	0.215	4.09E-05
Tubb3	3.51E-09	0.64687805	1	0.963	7.64E-05
Prdx2	3.78E-09	0.72277812	1	0.953	8.23E-05

Osbpl9	5.01E-09	0.83250073	0.913	0.813	1.09E-04
Fbxo17	5.56E-09	0.50343797	0.652	0.15	1.21E-04
Stbd1	6.55E-09	1.09297275	1	0.963	1.43E-04
Slc35b1	9.68E-09	0.68626655	0.957	0.738	2.11E-04
Rd3	1.35E-08	0.5858953	1	0.972	2.93E-04
Gchfr	1.35E-08	0.32772543	0.522	0.065	2.94E-04
Ppib	1.55E-08	0.6188014	1	0.972	3.38E-04
Selenof	1.55E-08	0.51120029	1	0.981	3.38E-04
Plxdc2	1.59E-08	0.2695123	0.435	0.037	3.45E-04
Ugp2	1.63E-08	0.90939627	0.957	0.794	3.56E-04
Tmed3	2.62E-08	0.50570554	1	0.916	5.71E-04
B2m	3.78E-08	1.26181829	0.913	0.542	8.23E-04
Akr1b3	6.06E-08	0.97983293	0.87	0.523	1.32E-03
Optn	7.24E-08	0.31830823	0.478	0.065	1.58E-03
Golim4	8.68E-08	0.52488666	0.913	0.551	1.89E-03
Selenom	1.04E-07	0.49334844	1	1	2.26E-03
Tppp3	1.17E-07	0.89025439	0.652	0.168	2.55E-03
Racgap1	1.58E-07	0.61403494	0.913	0.561	3.45E-03
Rhou	1.72E-07	0.39239137	0.609	0.15	3.74E-03
Dnajb11	1.76E-07	0.70097289	0.957	0.944	3.84E-03
Mfap3l	2.28E-07	0.28167932	0.565	0.103	4.96E-03
Kctd1	2.38E-07	0.88812556	0.913	0.542	5.17E-03
Traf3ip3	3.03E-07	0.73231367	0.391	0.037	6.61E-03
Galnt18	3.24E-07	0.55665364	0.826	0.411	7.05E-03
Calb2	3.73E-07	0.43308595	1	1	8.13E-03
Cdkn1a	3.82E-07	0.5373044	0.957	0.907	8.33E-03
Spcs3	4.63E-07	0.55754661	0.957	0.832	1.01E-02
Dusp26	4.98E-07	0.54873277	0.957	0.822	1.08E-02
Bri3bp	6.03E-07	0.36483009	0.522	0.112	1.31E-02
Vmn2r53	1.01E-06	2.68138046	0.217	0	2.21E-02
Spcs2	1.09E-06	0.59703272	0.957	0.944	2.37E-02
Carhsp1	1.32E-06	0.38531423	0.522	0.112	2.87E-02
Dclk1	2.00E-06	0.39895571	0.826	0.327	4.35E-02
Guk1	2.05E-06	0.5985497	0.913	0.897	4.45E-02
B230217C12Rik	2.24E-06	0.424191	1	0.813	4.87E-02

Supplementary Table S2

Significantly Up and Down Regulated Genes when Tfap2e/AP-2ε is ectopically expressed

Significantly Down-Regulated Genes

Gene Name	P. Value	Average Log Fold Change	Mature Basal %	Mature Apical %	Adjusted P.Value
Nsg1	1.05E-19	-1.026049429	0.978	0.991	2.28E-15
Ckb	3.16E-13	-0.832807392	0.957	1	6.89E-09
Plekhb1	1.02E-12	-0.66365877	0.804	0.991	2.23E-08
Calr	1.99E-12	-0.848017913	0.326	0.879	4.33E-08
Gng13	3.92E-11	-0.851799068	0.978	0.981	8.55E-07
Prdx1	6.92E-11	-0.670948424	0.674	0.925	1.51E-06
Ftl1-ps1	5.23E-10	-1.01755918	0.5	0.822	1.14E-05
Calm2	7.50E-09	-0.359436172	1	1	1.63E-04
Rps4x	9.27E-09	-0.462870937	0.978	1	2.02E-04
Chgb	5.21E-08	-0.509353353	0.63	0.907	1.13E-03
Obp2a	5.51E-08	-0.803452485	0.5	0.832	1.20E-03
Esd	1.16E-07	-0.447142323	0.391	0.748	2.54E-03
Eml2	1.21E-07	-0.290177152	0.152	0.645	2.63E-03
Lcn3	3.31E-07	-0.704072872	0.413	0.804	7.22E-03
Nqo1	4.44E-07	-1.080448365	0.239	0.636	9.68E-03
Ppp1r1a	6.98E-07	-0.395511356	0.935	0.953	1.52E-02
Id4	9.43E-07	-0.48810942	0.283	0.673	2.05E-02
Tspan1	1.12E-06	-0.469458509	0.543	0.785	2.45E-02
Cpe	1.20E-06	-0.310695303	1	1	2.61E-02
Gt(ROSA)26Sor	1.32E-06	-0.45231242	0.717	0.832	2.88E-02
Tstd1	1.35E-06	-0.387425488	0.935	0.963	2.94E-02

Significantly Up-Regulated Genes

Gene Name	P. Value	Average Log Fold Change	Mature Basal %	Mature Apical %	Adjusted P.Value
Abca7	2.79E-10	0.467733988	0.848	0.393	6.07E-06
Apmap	4.12E-08	0.499754357	1	0.916	0.000898417
Calb2	2.04E-08	0.32207374	1	1	0.00044526
Calr4	6.89E-11	0.580533012	0.935	0.916	1.50177E-06
Ccdc136	1.17E-08	0.433981247	0.696	0.252	0.000254306
Cdkn1a	2.88E-07	0.455507857	1	0.907	0.006262153
Cst6	3.50E-14	1.099290617	0.935	0.794	7.62225E-10
Dbi	3.62E-12	1.062519896	0.957	0.813	7.8747E-08
Dio3os	1.34E-15	0.383916442	0.652	0.047	2.92422E-11

Dlx4	8.01E-09	0.438918572	0.783	0.327	0.000174394
Dnajc3	5.15E-07	0.423663136	0.913	0.729	0.011213757
Dusp15	1.60E-08	0.288331862	0.587	0.14	0.00034899
Dync1i1	3.35E-08	0.495088228	0.848	0.533	0.000729768
Enpp1	1.92E-06	0.36206672	0.891	0.551	0.041912856
Fam3c	3.92E-07	0.381794339	0.913	0.664	0.008538247
Fbxo17	1.06E-17	0.668034836	0.804	0.15	2.31481E-13
Fmnl2	1.47E-06	0.294102212	0.717	0.346	0.031962548
Gm36028	1.51E-15	1.565013376	0.935	0.682	3.27889E-11
Gnao1	5.65E-07	0.344705173	0.783	0.327	0.012315414
Golim4	1.06E-06	0.393270819	0.804	0.551	0.023038974
Itpr1	1.54E-12	0.42801754	0.696	0.131	3.35489E-08
Jak1	1.57E-07	0.423690646	0.978	0.972	0.003418952
Kctd1	7.64E-16	0.85428255	0.978	0.542	1.66452E-11
Kctd17	5.75E-08	0.383015359	0.957	0.907	0.001251818
Khdrbs1	9.29E-07	0.388803088	0.935	0.692	0.020230178
Krt18	2.14E-06	0.448568282	0.935	0.673	0.046678066
Lrrc58	5.13E-09	0.336180339	0.717	0.243	0.00011176
Mab21l2	3.38E-11	0.342240813	0.37	0	7.3587E-07
Mapk8ip2	1.52E-07	0.38275929	1	0.963	0.003310007
Mfap3l	5.77E-11	0.330339336	0.609	0.103	1.25577E-06
Mfge8	7.50E-08	0.517438515	0.913	0.794	0.001634157
Mgat5	3.40E-07	0.328523537	0.87	0.486	0.007398101
Mt3	2.31E-12	0.486337274	0.761	0.215	5.03186E-08
Osbpl9	3.00E-09	0.615805448	0.957	0.813	6.544E-05
Pir	6.37E-09	0.572417884	0.848	0.486	0.000138796
Ptprd	4.71E-07	0.333394508	0.522	0.14	0.010266165
Racgap1	1.11E-06	0.405891754	0.87	0.561	0.024189968
Rims3	2.59E-07	0.430808566	1	0.916	0.005638623
Rmdn3	2.84E-08	0.443857099	0.783	0.458	0.000618452
Rpl11	2.14E-07	0.287691748	0.978	0.981	0.004668027
Smchd1	6.17E-13	1.30491047	0.935	0.598	1.34339E-08
Spats2	3.38E-12	0.613696552	0.957	0.832	7.36795E-08
Stbd1	1.62E-08	0.724116114	0.978	0.963	0.000353362
Suox	9.51E-08	0.433632116	0.739	0.364	0.002071784
Tafa1	1.26E-13	0.39251169	0.522	0.028	2.74227E-09
Tfap2e	7.33E-30	2.020231614	0.935	0.019	1.597E-25
Tsnax	2.00E-08	0.574771495	1	1	0.000435139